Flow Field Structure, Characteristics of Thermo-Hydraulic and Heat Transfer Performance Analysis in a Three Dimensions Circular Tube with Different Ball Turbulators Configurations

Dr. Ahmed Ramadhan Al-Obaidi[1] **Prof. Dr. Issa Chaer[2]**

[1]Department of Mechanical Engineering, Faculty of Engineering, Mustansiriyah University, Baghdad, Iraq.

[2]Director of Enterprise, School of The Built Environment and Architecture, London South Bank University, London, UK.

[3]Corresponding Author E-mail: ahmedram@uomustansiriyah.edu.iq

Abstract

This paper presents the findings from a research study using computational fluid dynamics (CFD) on the impact of different diameter Ball Tabulators Inserts (BTI) on the three-dimensional flow pattern and heat transfer characteristics within a circular tube. This analysis was carried under uniform heat flux conditions with different BTI diameters (1, 2, 3, 4, 5, 6, 7, and 8 mm). Fluid flow, pressure drop, dynamic pressure, velocity components, thermo-hydraulic, turbulent kinetic energy, and turbulent viscosity were analysed qualitatively and quantitatively. The performance evaluation results revealed that the characteristics of flow behaviour and the velocity field contours variations are closely associated to the BTI configurations. Also, the computational results indicated that the change in fluid flow velocity near the pipe wall and around the BTI are important parameters for the heat transfer enhancement as compared to that obtained without BTI under the same conditions. Moreover, using BTI presented a distinguished influence on the rate of heat transfer. Additionally, vortex flow through means of this kind of BTI is an important parameter in the enhancement of heat transfer. The use of BTI can enhance the rate of heat transfer performance by more than 46 %. Furthermore, the maximum value for the PEF is found to be more than 1.03.

Keywords: Flow structure, thermo-hydraulic flow, heat transfer performance, ball turbulators, CFD

1. Introduction

Heat exchangers are employed extensively in different industrial applications and their effectiveness forms an important factor of the overall process performance. Thus, many industries and researchers have attempted to develop different approaches and techniques to enhance heat transfer in heat exchangers. In general heat transfer enhancement techniques can be divided into two main categories namely active and passive techniques [1,2]. Those which require an external power source to maintain the enhancement mechanism are named active methods. Examples of active enhancement methods are stimulating the fluid or vibrating of the surface. While passive techniques do not require direct input of external power. Augmentation is achieved by use of inserts or by surface or geometrical modifications. This promote higher heat transfer coefficients by altering the existing flow behaviour. In this case, additional indirect power may be required to overcome any increase in the fluid pressure drop as a result of the passive techniques. A variety of heat transfer devices and shapes have been used in the case of inserts in tubes and channels such as wire coils, twisted bands, twisted tape inserts, [3-4]. All these approaches need more power demand for pumping the liquid [5-7]. Twisted tape inserts are the most usually employed in different fields due to their steady performance and simple shape [8-9]. However, the manufacturing complexity and increase in pressure drop is a disadvantage resulting from the use of this kind of turbulence promoter. The advantage gained in terms of the increase of average heat transfer coefficient by using this kind of turbulence promoters can be partially offset by the increased pumping power requirements. The use of ball turbulator inserts offers a simple flow augmentation alternative that can easily be used in heat exchangers and existing channels. Unfortunately, there is a lack of detailed analyses on this kind of device inserts in the available literature. Hence, this work was carried out, using numerical simulation using CFD, to predict the flow and heat transfer characteristic as a result of using a ball turbulator insert (BTI). CFD is widely applied in many fields such as fluids, air condition and heat transfer [10-12]. Many types of research have conducted heat transfer augmentation using different devices, for example, research work conducted by Patil and Deshmukh [13] studied the enhancement of heat transfer in a circular channel by using almond shaped dimples. They applied staggered array dimples in a circular tube and reported enhanced thermal performance by more than 66% as compared to the configuration of aligning dimples. Also, the results revealed that high heat transfer occurred near the dimples downstream because of flow reattachment. The heat transfer coefficients rise when the Reynolds number increases. Hosseinnejad et al [14] researched the effect of twisted tape on flow characteristics in the heat exchanger. The Nusselt number rises as the twisted tape torsion ratio decrease at higher Reynolds numbers. Hence, heat transfer can improve as compared to a smooth pipe. Abraham and Maki [15] conducted hydrodynamics of laminar flow in pipes using dimples. They were simulated varied dimple diameters between 0.125 and 2mm inside tube diameter of 6 mm. For small dimple diameters, the results found that the liquid does not enter into dimples for forming recirculation area. However, as the dimple diameters increase the flow moves in the downstream direction, and the recirculation region forms. Moreover, the flow behaviour around the dimples was related to the hydrodynamic resistance changes. Vignesh et al. [16] researched heat transfer in a heat exchanger with concentric dimple pipe. They observed that the overall heat transfer coefficient inside and outside pipe was more than concentric plain pipe by about 56 to 64%. Also, the effectiveness parameter was more than concentric plain pipe by around 55%. Promthaisong et al. [17] studied the influence of different configuration parameters on behaviours of heat transfer and turbulent flow using triple start corrugated pipes. In their work, results point out that using corrugated type triple-start can produce more helical swirl flow and swirl flow and hence that leads to decrease the thickness of thermal boundary layer and improve the rate of heat transfer in pipes. The friction factor was increased as the values of corrugated depth increase and values of corrugated pitch decrease. Van et al. [18] evaluated the heat transfer performance using helically corrugated pipes type. The results indicated that using the latter type can improve heat transfer by about 83 to 119% and the pressure losses cost were around 5.6 to 6.7 times as compared to the bare tube. The potential energy conversion in the pressure form into TKE (turbulent kinetic energy) was contributed to the turbulent flow mixing. Akansu [19] investigated pressure drops and heat transfers in a circular pipe using porous ring turbulators. Author numerically calculations were carried out by applying the Fluent code with SST (shear stress transport) model. The results found that the heat-transfer decreases as the ratio of pipe length per inside pipe diameter (L/D) increase. Also, the high Nusselt number happened when L/D equal 1, Reynolds number increased when the friction factor decreases. At maximum L/D ratios, the higher recirculation areas occurred. Sharma et al. [20] analysed heat transfer inside the circular tube using the various orientation of insert based on CFD. Results revealed that as insert orientations changed the outlet temperature reduces with Reynolds number rise. Using inserts orientation leads to outlet temperature increases by about 107 to 126% as compared to the smooth pipe (without insert). Also, the heat transfer coefficient increases as the Reynolds number increases. Yuan et al [21] conducted the turbulent flow characteristics, friction factor, and heat transfer in a circular pipe using ball turbulators. They analysed flow with a range of Reynolds number from 5000 to 35,000 with of constant heat flux condition. They noticed that the rate of heat transfer using ball turbulators was increased about 1.26 to 2.01 times as compared to the plain pipe. Also, the friction factors were increased from 34.6 to 46.2%. The flow velocity closed the pipe wall is highly enhanced as used ball turbulators. Afshari et al [22] numerically analysed the flow and heat transfer in heat exchanger tube using ball turbulators type. They observed that using ball turbulators at a low Reynolds number can have higher vortex flow generation and hence further effective heat transfer performance can be improved. Maximum Nusselt number was enhanced around 43% when used balls as a compared smooth tube. Generally, based on the literature survey above, it can be noticed that the majority of studies were associated with simple, twisted, and corrugated insert tapes positioned in the tube. Conversely, there are few investigations related to turbulising part inserts placed in the axial flow direction of the pipe, such as that carried out in this analysis. Ball turbulators type with different geometrical configurations in this study is used as an effective technique in heat exchangers pipes. Firstly, the numerical results are validated with available experimental data. Secondly, all cases are simulated using the Fluent CFD based method after that the obtained outcomes are investigated and discussed in terms of static pressure, dynamic pressure, axial velocity, radial velocity, tangential velocity, static temperature, turbulent kinetic energy, and turbulent viscosity in qualitative and quantitative analyses. According to obtained results, characteristics of fluid flow and enhancement of heat transfer of the ball inserts in three dimensions circular pipe are investigated.

2. Numerical Modelling of Geometrical Model

Figure 1, shows a 3D schematic of the circular pipe with BTI, the pipe total length is 1920 mm and pipe diameter is 11.08 mm, respectively. This figure illustrates the geometry of the three-dimensional pipe model, and this numerical investigation is conducted for various diameters of the BTI configurations namely 1, 2, 3, 4, 5, 6, 7, and 8 mm diameters. The distance gap between each of the balls insert is simultaneously constant for different ball diameters in the numerical domain length. The working fluid flow is water. The value of heat flux is approximately constant 800 W/m^2 supplied on the external pipe wall. Fully developed flow and steady state conditions for all computational simulations are carried out.

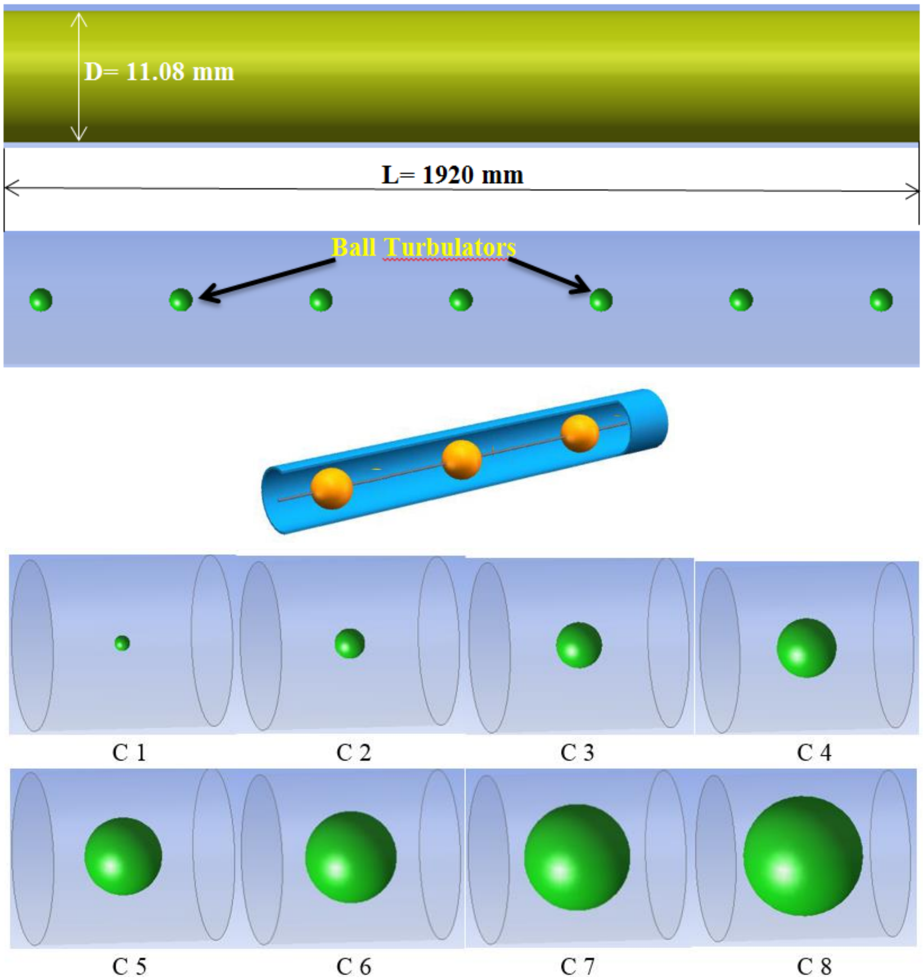

Figure 1: The 3D view pipe computational domain with different ball elements insert

2.1. Meshing Flow Domain and Grid Generation Independence Test

Firstly, before the start of the numerical simulations, a variety of mesh densities were generated for different configurations. Tetrahedral cell mesh was used for generation mesh [23]. The shape was used to mesh the flow pipe domain and ball inserts as illustrated in Figure 2. Also, in the mesh domain, the system of the boundary layer near the pipe wall was used in order to obtain accurate numerical results. ANYSYS

ICEM was employed to create the flow meshes, the grid refinement rule is applied, the adaptive grid refinement is also carried out in this numerical model. In order to achieve the numerical solution reliability for pipe with ball turbulator insert analysis of grid independence were carried out.

The grid independence test is carried out to find the best structure of mesh in terms of time cost consumption and accuracy results. These independence grid tests are conducted for both smooth pipe and pipe with ball turbulators. For each pipe (smooth and with ball turbulators), eight numbers of grids where the grids ranging from 500000 to 3100000 are carried out for the Nusselt number (Nu) and friction factor (f) values. Table 1 summarises the percentage of errors in Nu and f against mesh elements. The results established a good compatibility compared to available experimental data carried out by Albanesi et al. [25] with a average deviation around 2.1% for the Nu and 2.5 % for f.

Table 1: Investigation of mesh independency

No. of element	Smooth Pipe		No. of element	Ball Turbulator Pipe	
	Nu	f		Nu	f
	(%)	(%)		(%)	(%)
501245	5.2	6.3	625487	5.4	6.7
802578	4.6	5.2	987584	4.8	5.5
1125784	4.1	4.5	1205487	4.2	4.8
1502487	3.2	4.1	1752461	3.5	4.2
1901548	2.8	3.8	2015487	3.1	3.9
2354622	2.3	2.5	2365782	2.5	3.1
2568794	2.1	2.3	2797542	2.2	2.8
3054687	1.9	2.1	3102458	2.01	2.5

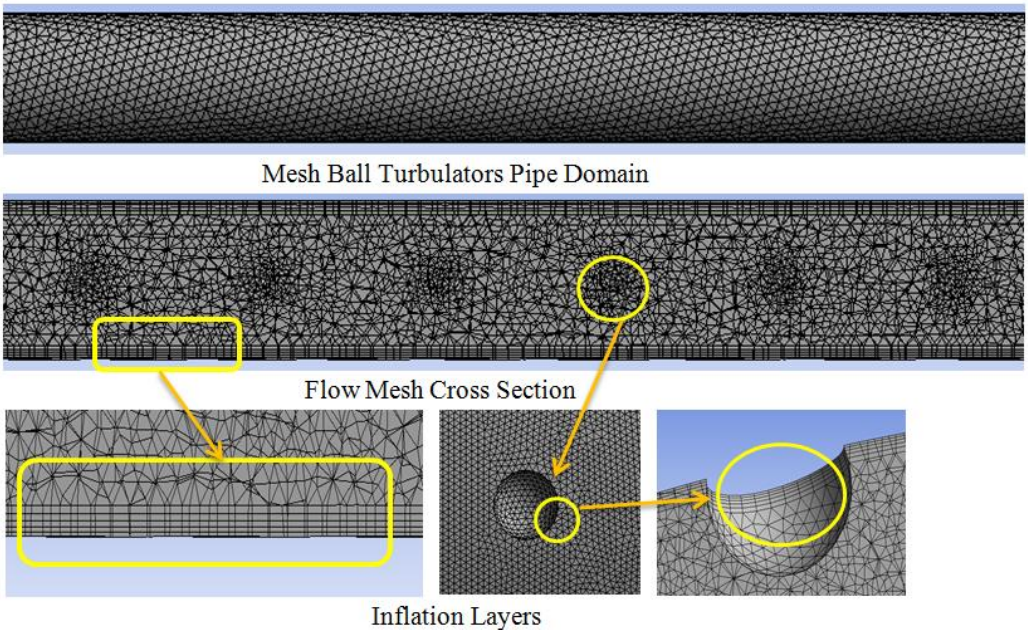

Figure 2: Mesh for flow domain generation of the pipe with ball geometry

For the solution method, the pressure–velocity coupling scheme is chosen. Momentum, continuity, and energy equations were applied to solve the pressure drop and heat as well as the different fluid features in CFD methods solver, 3D double-precision version was also used. As mentioned earlier, the CFD methods were used in this current numerical investigation. Entire equations for fluid flow accompanied by the specified conditions were calculated in the method of finite volume. The turbulent kinetic energy (TKE), momentum, continuity, and rate of turbulent dissipation were modeled by the scheme of 2nd order upwind. The algorithm of semi-implicit SIMPLE was adopted for the computational simulation procedure. The relative residuals convergence criterion for different variables comprising pressure, various velocity components, mass flow, temperature, rate of turbulent dissipation, TKE, and energy less than 10^{-7} were applied.

Primarily, the following equations of continuity, momentum, and energy are specified:

mass conservation equation:

$$\frac{\partial \rho}{\partial t} + \frac{\partial}{\partial x_i}(\rho v_i) = 0 \tag{1}$$

Where, t, v, and ρ are time, velocity, and density.

Momentum equation:

$$\frac{\partial}{\partial x_j}(\rho v_i v_j) = \frac{-\partial P}{\partial x_i} + \frac{\partial}{\partial x_j}\left[\mu\left(\frac{\partial v_i}{\partial x_j} + \frac{\partial v_j}{\partial x_i}\right) - \frac{2}{3}\mu\frac{\partial v_k}{\partial x_k}\delta_{ij}\right] \tag{2}$$

Where, i, j, k, P, and μ are velocity directions in X, Y, and Z, pressure, and Dynamic viscosity.

The energy conservation law:

$$\frac{\partial}{\partial t}(\rho e) + \frac{\partial}{\partial x_j}\left(\rho v_j c_p T - k\frac{\partial T}{\partial x_j}\right) = u_j\frac{\partial p}{\partial x_j} + \left[\mu\left(\left(\frac{\partial v_i}{\partial x_j} + \frac{\partial v_j}{\partial v_i}\right) - \frac{2}{3}\frac{\partial v_k}{\partial x_k}\delta_{ij}\right)\right] \tag{3}$$

Where ρ, μ, c_p, u, P, and T are fluid density, dynamical viscosity, specific heat coefficient, fluid velocity, pressure, and temperature respectively. The numerical system is modeled in 3D steady-state with RNG k–ε turbulence model is chosen for computational solutions. The equations of k–ε is associated with this turbulence model are given as follows [24]:

$$\frac{\partial}{\partial t}(\rho k) + \frac{\partial}{\partial x_i}(\rho k v_i) = \frac{\partial}{\partial x_j}\left[\left(\frac{\mu + \mu_t}{\sigma_k}\right)\frac{\partial k}{\partial x_j}\right] + \mu_t\left(\frac{\partial v_i}{\partial x_j} + \frac{\partial v_j}{\partial v_i}\right)\frac{\partial v_i}{\partial x_j} - \rho\varepsilon \tag{4}$$

$$\frac{\partial}{\partial t}(\rho\varepsilon) + \frac{\partial}{\partial x_i}(\rho\varepsilon v_i) = \frac{\partial}{\partial x_j}\left[\left(\frac{\mu + \mu_t}{\sigma_\varepsilon}\right)\frac{\partial \varepsilon}{\partial x_j}\right] + C_{1\varepsilon}\frac{\varepsilon}{k}\mu_t\left(\frac{\partial v_i}{\partial v_j} + \frac{\partial v_j}{\partial v_i}\right)\frac{\partial v_i}{\partial v_j} - C_{2\varepsilon}\rho\frac{\varepsilon^2}{k} - \alpha\rho\frac{\varepsilon^2}{k} \quad (5)$$

$$\mu_t = \rho C_\mu \frac{k^2}{\varepsilon} \quad (6)$$

The fluid flow (k) local thermal conductivity is obtained through applied the mean bulk temperature in the below equation.

$$T_b = (Tout + T_{in})/2 \quad (7)$$

Where, Tb, Tout, and Tin are bulk temperature, outlet, and inlet temperatures.

The computed of Reynolds number in the pipe using equation (8)

$$Re = \frac{\rho v d_e}{\mu} \quad (8)$$

Where d_e is pipe effective diameter.

The friction factor across the pipe can be written as follows:

$$f = \frac{\Delta P}{(L/D)(\rho v^2/2)} \quad (9)$$

Where L and D are the pipe length and diameter

The pipe effective diameter equation is calculated written as:

$$d_e = \sqrt{\frac{4(V_{\text{tube}} - V_{\text{turbulator}})}{\pi L}} \quad (10)$$

The rate of heat transfer given in a condition of steady state is written as:

$$Q = \dot{m}_w C_{p\_}(T_{out} - T_{in}) \quad (11)$$

Where $\dot{m}_w$ and C_p mass flow and specific heat.

Nusselt number formula can be determined by equation (12):

$$Nu = \frac{\text{h d}}{\text{k}} \quad (12)$$

Where k, h, and d were the fluid thermal conductivity. heat transfer coefficient and pipe diameter

The performance evaluation factor (PEF) ratio is used to enhance overall pipe performance which can be determined using equation (11):

$$PEF = \frac{Nu/Nuo}{f/fo} \quad (11)$$

Where fo and Nuo are the smooth pipe friction factor and Nusselt number.

2.2. Boundary Flow Conditions

In the current numerical work, the boundary conditions included a constant temperature condition on the pipe wall. At the inlet pipe, temperature profiles and fully developed flow velocity inlet are used. Moreover, at the outlet pipe, a boundary condition pressure outlet is applied. Figure 3 describes the circular pipe with different ball turbulators inserted physical numerical model which used in this investigation.

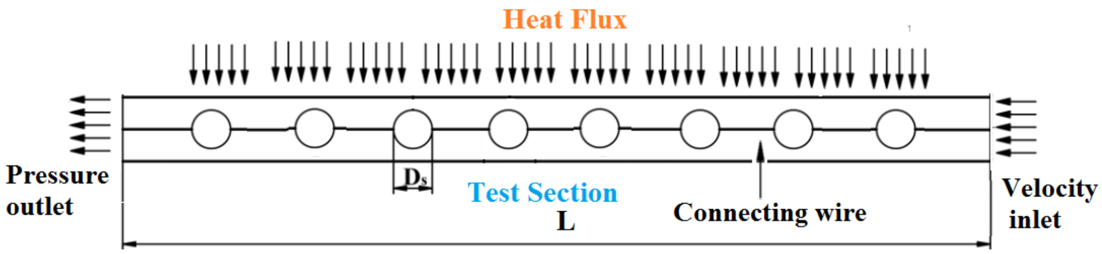

Figure 3: Circular pipe with ball turbulators inserted physical numerical model

3. Numerical Results Validation

In order to verify the numerical results technique defined above, initial numerical calculations were performed and the results of heat transfer rate were compared with available experimental data carried out by Albanesi et al. [25] as illustrated in Figure 4. As could be seen from this figure, the heat transfer rate results obtained from the CFD calculation at different flow rates compare well with the experimental ones available in the literature. The maximum deviation between the simulated and actual results is less than 7%.

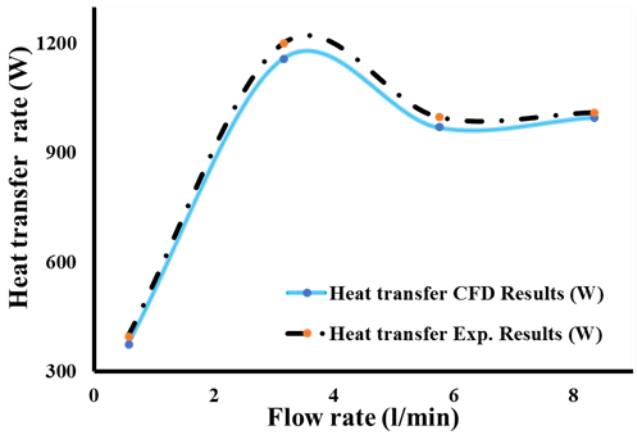

Figure 4: Numerical simulation valuation results

The pipe test section in this numerical investigation is divided into seven plane positions as represents in Figure 5 in order to obtain more information details for flow structure and performance of heat transfer.

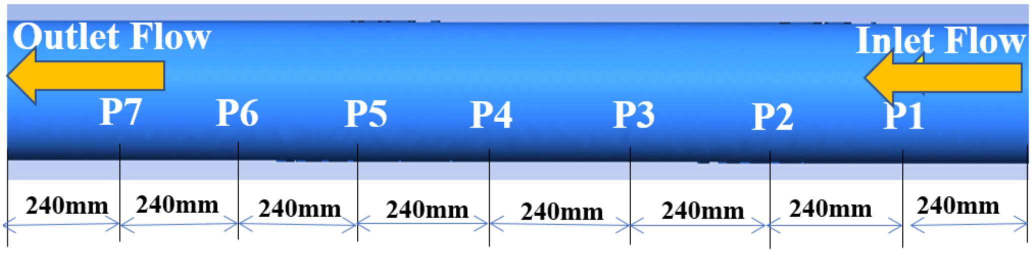

Figure 5: Pipe test seven planes

4. Results and Discussion

The next section analyses and discuss the flow field results in the pipe in terms of static pressure, dynamic pressure, and velocity components in quantitatively and qualitatively analyses.

4.1. Characteristics of Flow Structure Analysis

Figure 6 represents the static pressure contours in the plain pipe longitudinal sections for seven different plane sections. The pipe design parameters are pipe length of 1920 mm and pipe diameter of 11.08 mm. The operating flow condition is the temperature of 313.15 K, the flow of 0.56 l/min, and the heat transfer coefficient of 800 W/m^{2}K. As could be seen from the figure, the high pressure is concentrated nearby the inlet zone as illustrated by the inlet plane and the pressure along the pipe decreased with increasing distance. The results indicate that this observation for pressure was the same for all cases under different ball turbulator diameters as listed in Table 1. By analysing this table, it can be noted that as the ball diameters increase the pressure also increased.

Table 1: statistic pressure change with different ball turbulator diameters

Plane	D_1	D_2	D_3	D_4	D_5	D_6	D_7	D_8
-	1 mm	2 mm	3 mm	4 mm	5 mm	6 mm	7 mm	8 mm
Pressure in	126.93	139.21	179.53	232.14	314.32	474.05	737.36	1293.45
P1	109.63	139.21	156.29	202.40	274.27	474.05	643.39	1131.04
P2	93.97	120.84	133.97	173.48	235.06	413.56	551.29	969.57
P3	78.28	103.51	111.70	144.50	195.84	354.45	459.42	807.07
P4	62.54	86.27	89.39	115.54	156.64	295.15	367.52	644.57
P5	46.87	69.01	67.04	86.57	117.46	236.01	275.59	483.30
P6	31.21	51.68	44.67	57.67	78.18	176.95	183.68	322.20
P7	15.56	34.38	22.28	28.77	38.99	117.87	91.72	160.55
DP/L	0.066	0.072	0.093	0.1209	0.163	0.246	0.384	0.673

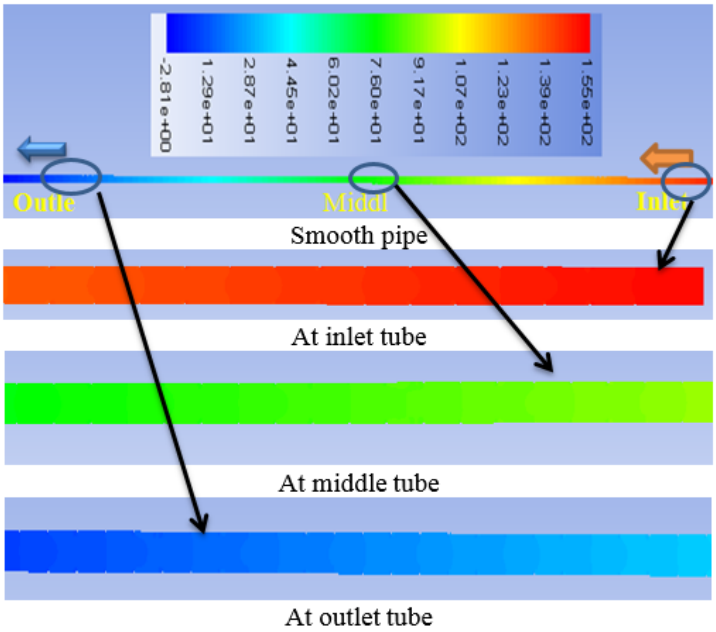

(A)

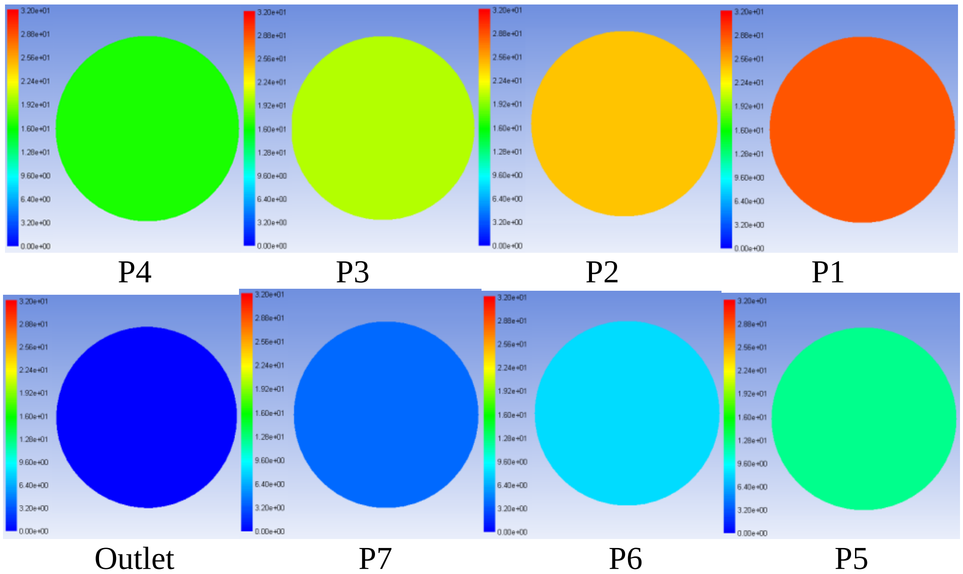

(B)

Figure 6: Static pressure in the pipe at different plane positions

Figure 7, presents the value of static pressure change between each plane with different ball diameters starting from 1 to 8 mm in the pipe with the same above figure pipe design parameters and flow conditions. The entire figures characteristic in this figure assigned and keep the similar scale for the particular type of diagram for comparison analysis purpose. It is evidently noted that the pressure in the pipe with the balls increased as the ball diameter increased. The maximum pressure took place with case C 8 i.e. with a ball diameter of 8 mm. Due to the size and location of these balls, more mixing and thus was generated and thus more vortex flow that lead to the disturbance of the thermal boundary layer.

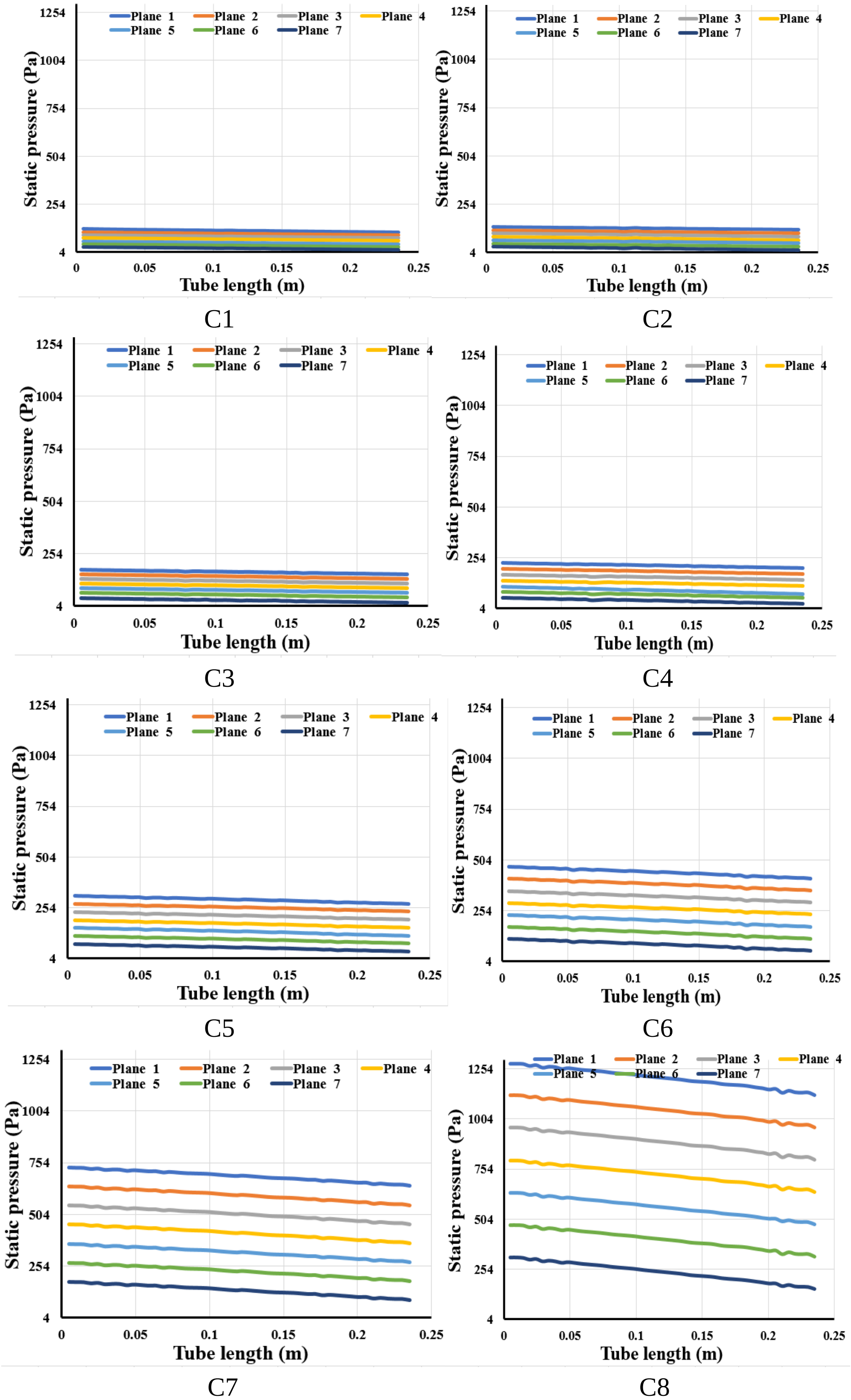

Figure 7: The change in static pressure profiles at different ball diameter

Further investigation of the change in static pressure, Figure 8 shows the effect of a variety of ball diameters on the static pressure using different statistical parameters including A) minimum, B) maximum and C) average pressure values. By analysing this figure, it can be observed that the behaviour of pressure has the same trend for all the above features. This means as the ball diameter increases the pressure also increases and the highest pressure takes place at plane 1 for all cases and planes under study.

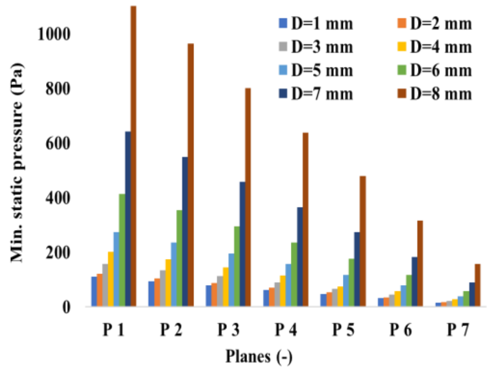

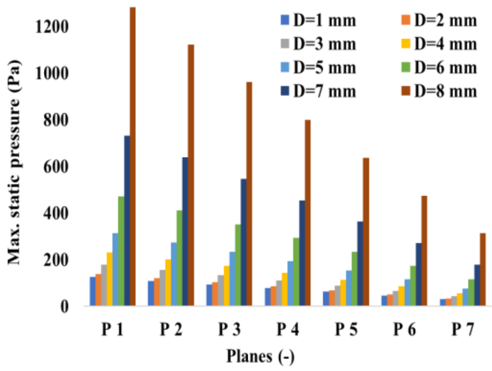

A B

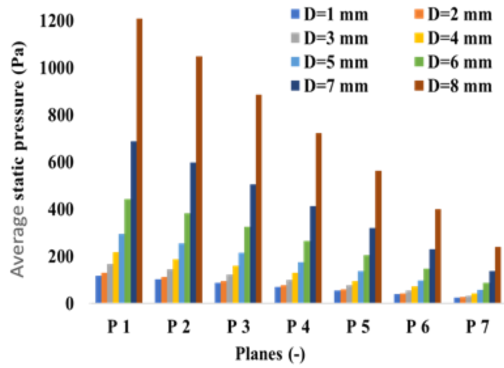

C

Figure 8: Analysis static pressure using different features

Figure 9 A and B illustrate the effect of balls on the change of dynamic pressure contours in both axial and radial sections, the results revealed that the dynamic pressure field changes as the ball diameter changes. The high pressure takes place between the ball's outer diameter and the pipe wall for all cases under analyses. Also, the low effect was for case 1 and the high effect was for case 8. At the same operating conditions, the numerical results clearly indicated that the pressure flow of fluid near the pipe wall with BTI is significantly enhanced. As observed that the maximum pressure seems near the pipe wall area instead of the central pipe area. This increase in dynamic pressure gradient can affect inducing the distribution of intense flow due to cause more mixing flow and hence leads to enhance the heat transfer rate between the flowing liquid and the pipe wall regions.

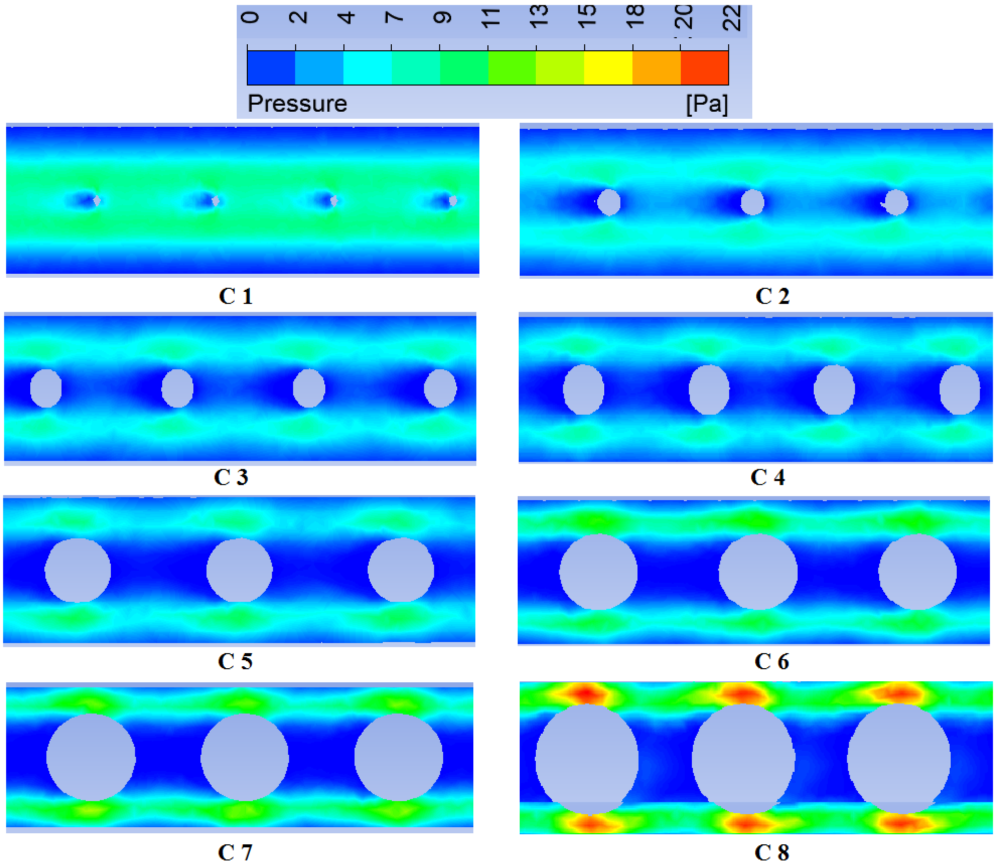

A) Dynamic pressure in axial flow sections

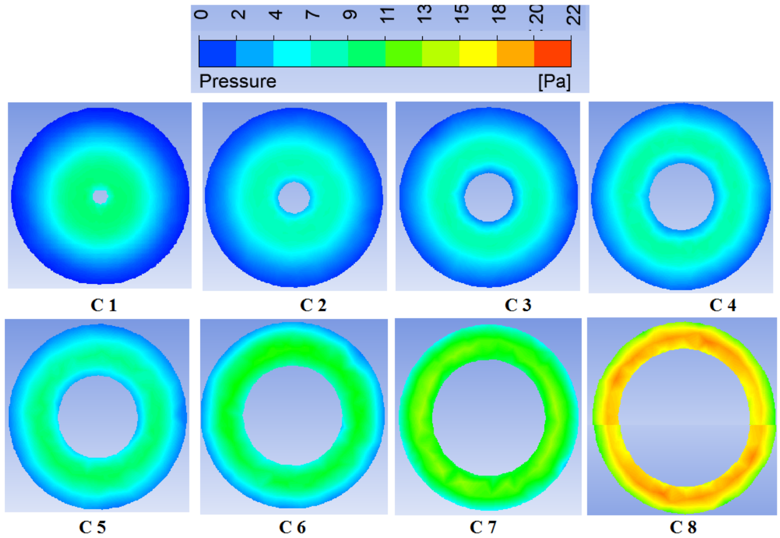

B) Dynamic pressure in radial flow section

Figure 9: The change in dynamic pressure in axial and radial flow directions

Figure 10 describes the change in curves of dynamic pressure profiles at a variety of ball configurations. As obviously noticed that these curve profiles are non-uniform for all cases under study and the results revealed that the ball highly affects the shape and value of these cuvees particularly at case C 1 because it has a high ball diameter. It is evidently noted that the value of the dynamic pressure profile increases near the pipe wall then it decreases closed the pipe center. However, at the pipe center region, the value of profiles decreases as the ball diameter increases for all planes. Moreover, the disturbance of the boundary layer is highly intensified through the use of BTI. The relevant intensity rises with the ball diameter increase. Hence, the friction factor rises, and boundary layers in flow become thinner at a higher value of ball diameter, and hence the rate of heat transfer increases as well. In general, due to the pipe under study contains a series of small balls connected with each other by a thin wire. Hence, due to the movement of the fluid in the flow direction causes an unusual or unstable movement of the balls, which causes them to move to the right or the left, causing this difference in figures.

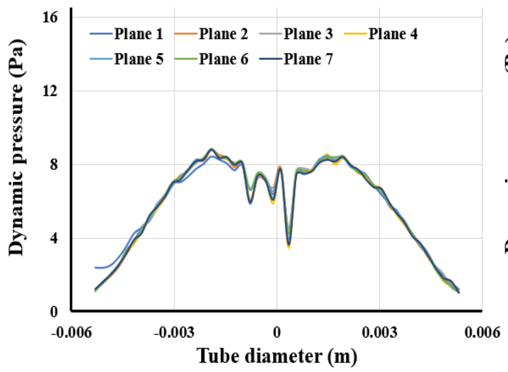

C1

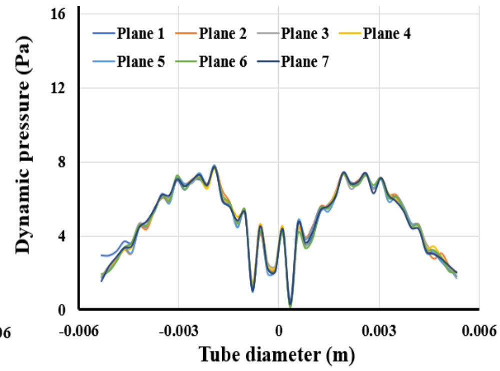

C2

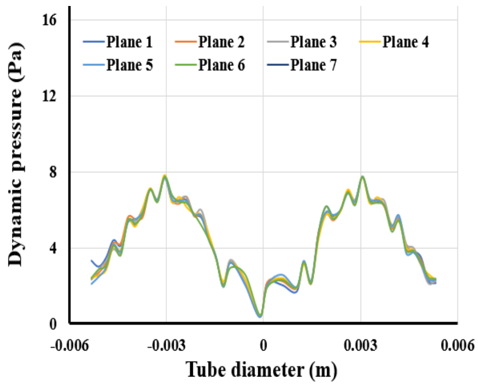

C3

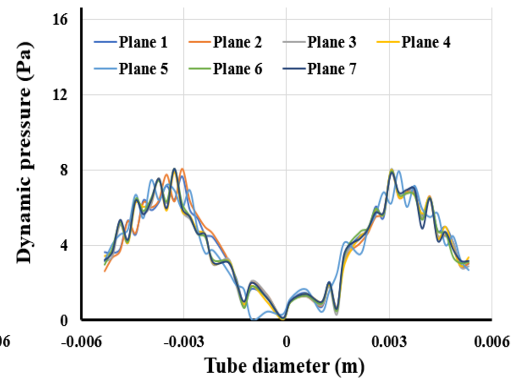

C4

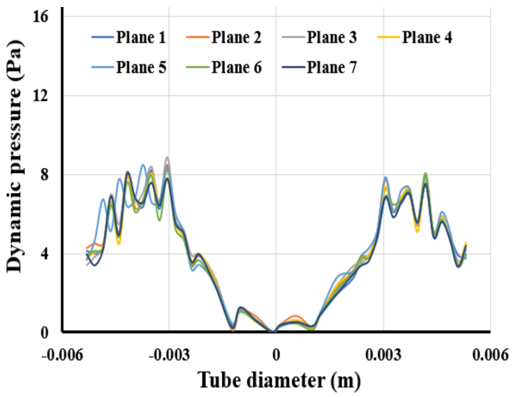

C5

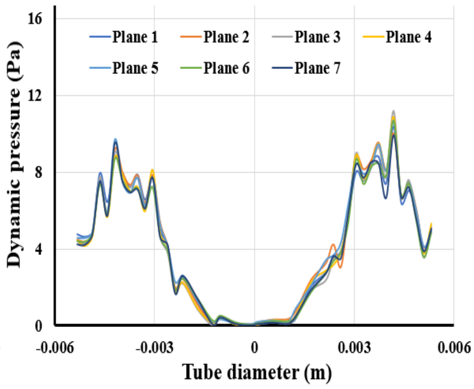

C6

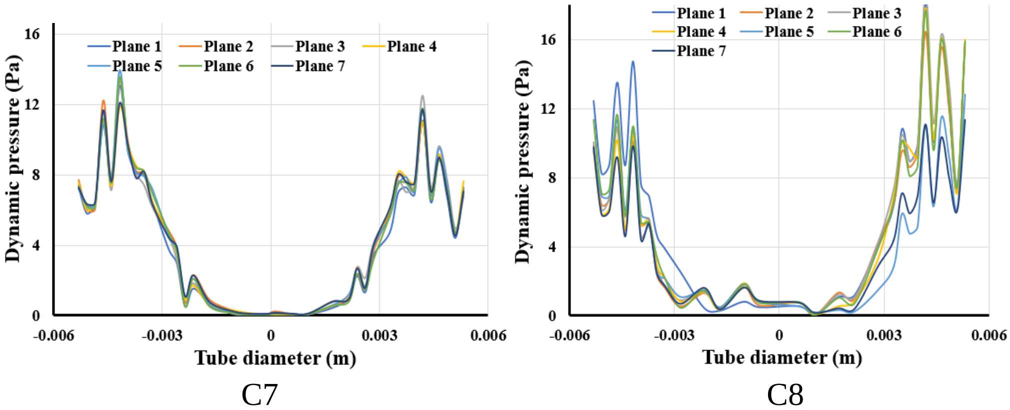

Figure 10: Dynamic pressure profile alteration at various ball configurations

Figure 11 A and B illustrates the axial flow velocity in both directions (axial and radial). The result noted that the flow velocity changes in the pipe as the ball configurations change. Also, the value of velocity increases around and between the outer ball diameter and the pipe wall regions. This change in velocity leads to higher flow resistance in the flow direction than in the boundary layer the velocity gradient increases. Hence, that leads to periodically disturb in the flow boundary layer and generate a distribution of intense turbulence periodically. That means it is useful to improve the rate of heat transfer between the outer ball region fluid flow in the pipe wall. Figure 11 C depicts the velocity vector under different ball diameters. As observed that the flow in the pipe is changed as the ball diameters increase. The higher value of the velocity vector occurs near the outer ball surfaces. These changes in flow behaviour inside the pipe due to insert the ball can cause more mixing and rotating flow and hence that leads to enhance the heat transfer in the pipe.

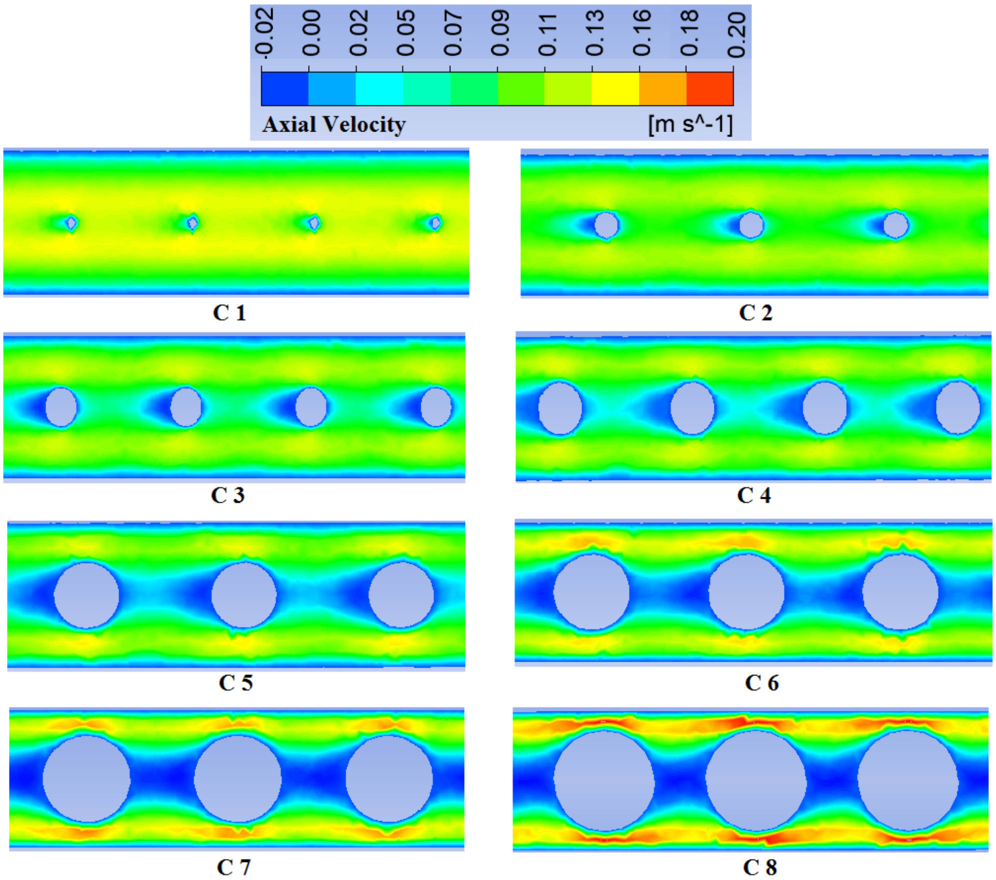

A) Axial velocity in axial flow direction

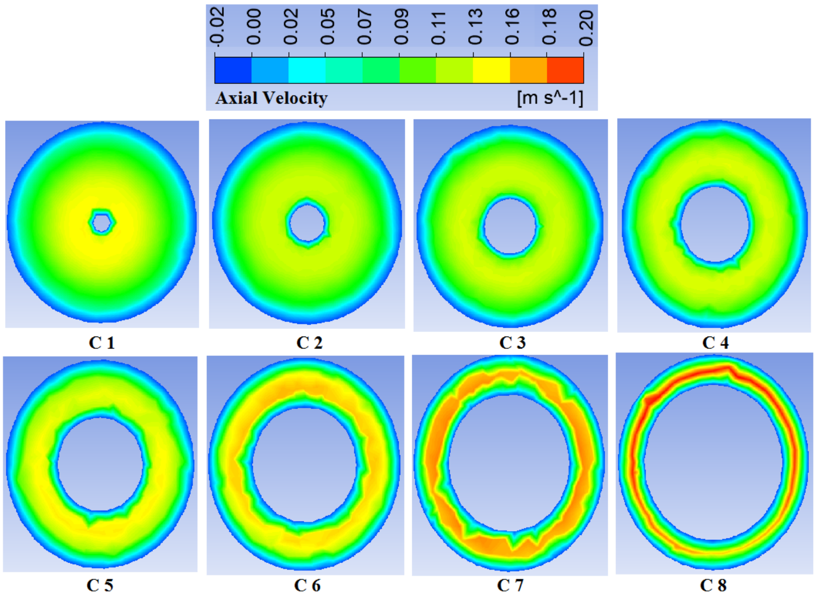

B) Axial velocity in radial flow direction

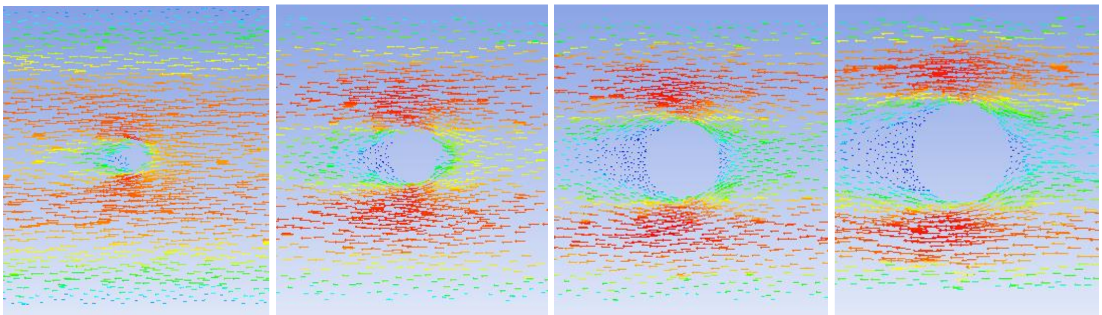

D= 1 mm D= 2 mm D= 3 mm D= 4 mm

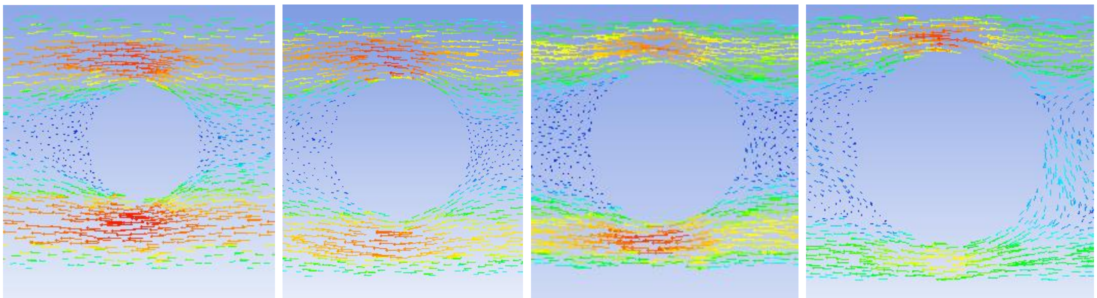

D= 5 mm D= 6 mm D= 7 mm D= 8 mm

C) Velocity vector at varying of ball daimeters

Figure 11: Axial flow velocity in different flow directions

Figure 12 describes the axial velocity profiles at different ball diameters, as observed from this figure all curves are non-uniform shaped especially nearby the pipe center due to the effects of balls, and the value of non-uniform shape decreases as the ball diameter increases. The influence of BTI configurations is greatly disturbed and intensified the boundary layer and as the ball diameter increase, the relevant intensity rises. That leads to the boundary layer flow within the flow direction becomes thinner as well as the friction factor rises at higher ball diameter then the rate of heat transfer enhances and increases.

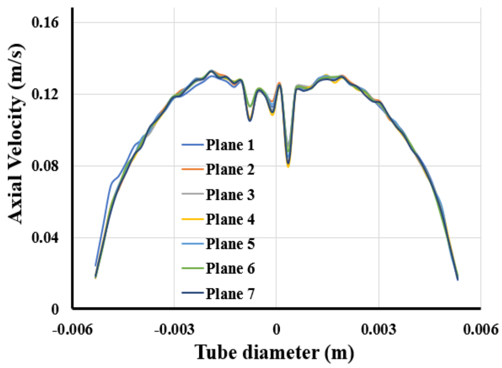

C1

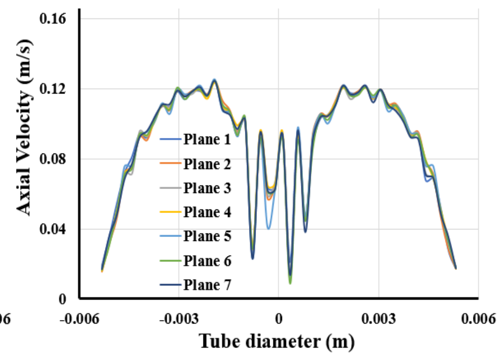

C2

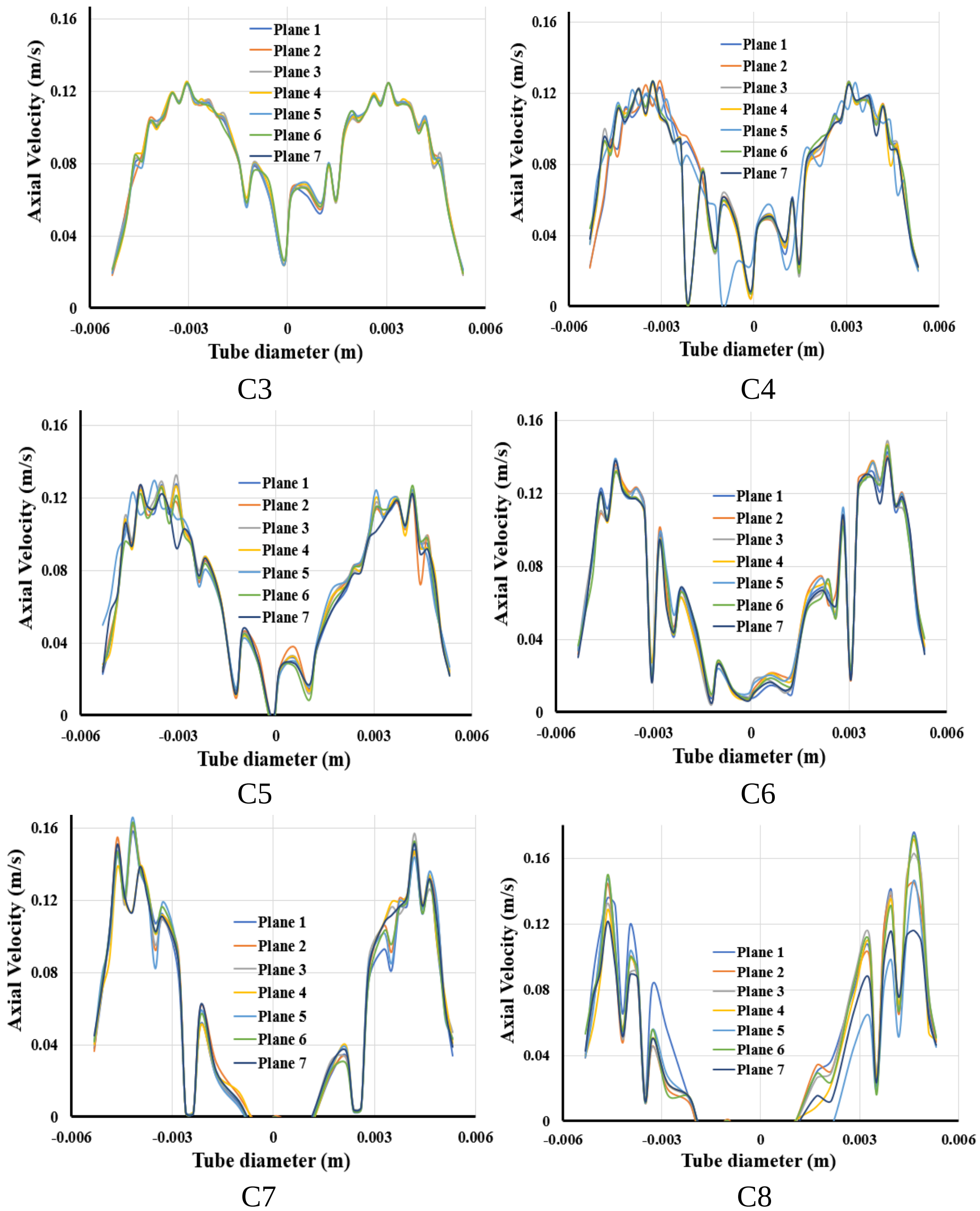

Figure 12: Curves of axial velocity profiles

For deep investigation regarding flow patterns, Figure 13 demonstrates the radial flow velocity fields. As noticed in this figure there is highly effective of the ball on the radial velocity, especially at higher ball diameter configuration. It is observed that these influences are near and around the ball flow. Moreover, as seen that in previous figures using BTI configurations can capable of changing and disturbing the boundary layer then it is caused more disturbance in the fluid. Consequently, both the flow resistance and rate of heat transfer will increase as the ball diameter increase due to more mixing of the flow and more vortex, and hence this result was agreed with Refs. [8 and 13].

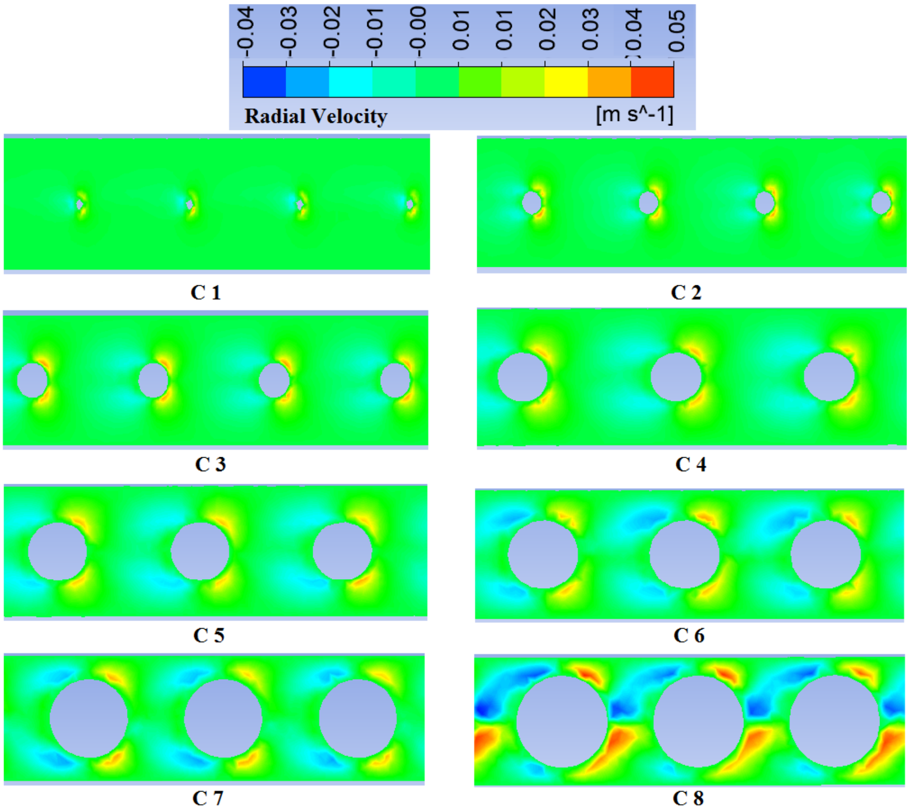

Figure 13: Axial flow velocity field at various ball diameters

The curve profiles of radial velocity in the pipe test sections of the improved pipe are illustrated in Figure 14 for various ball diameters. The results revealed that the value and profile shapes are changed and increased as the ball configurations increase especially at higher ball diameter these results are agreed with the above figure results. Moreover, this happened due to the high increase in the friction resistance is occurred and it goes up as well reaches to the higher value at balls with the larger diameter, and hence this result was agreed with Refs. [14 and 18].

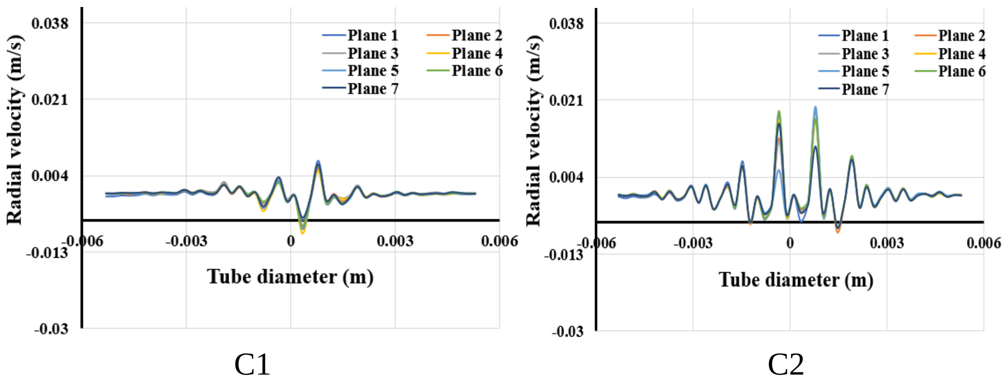

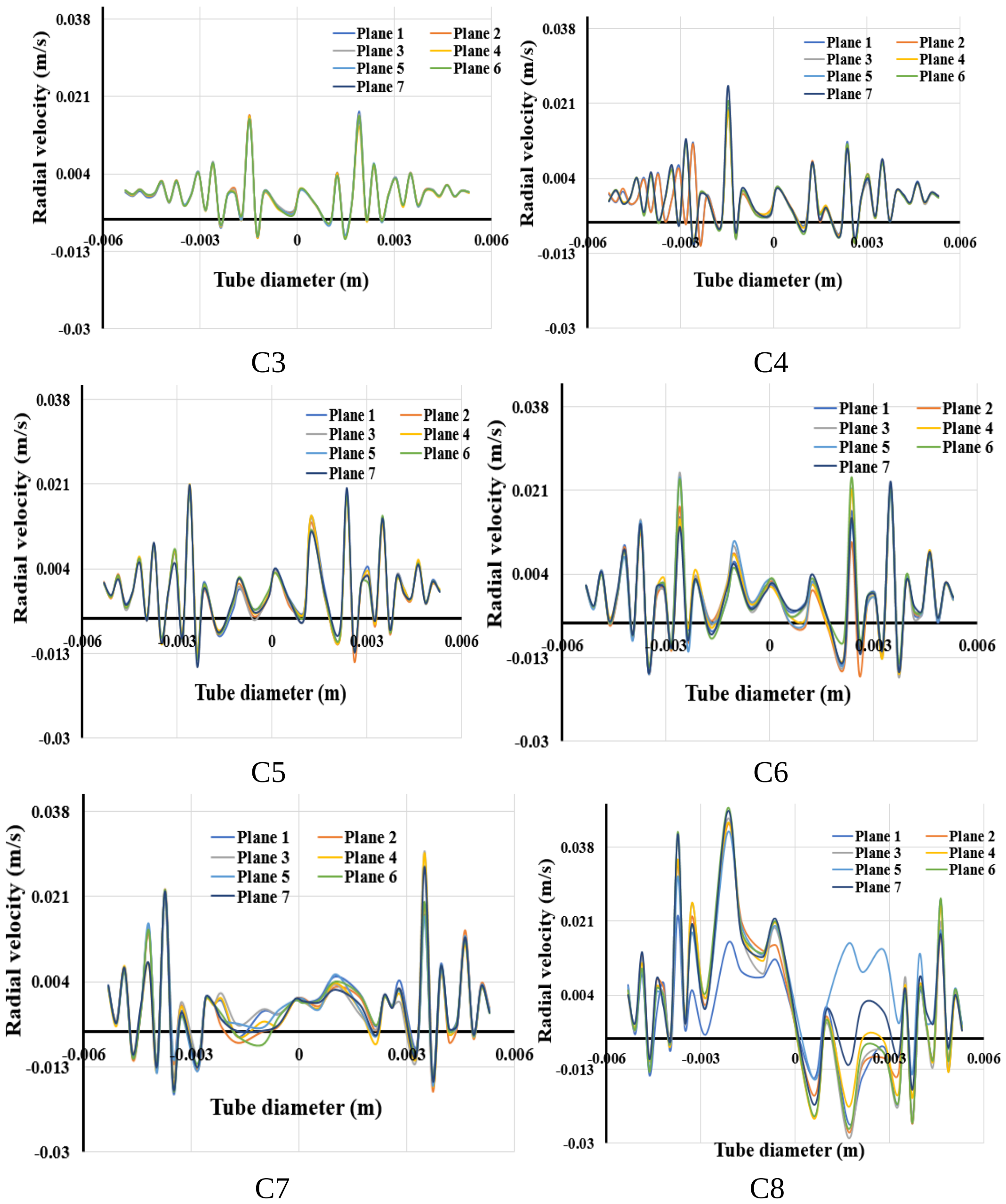

Figure 14: Curves of radial velocity profiles in the pipe at different planes

The contours of tangential flow velocity in the test pipe sections are shown in Figures 15 A and B. Numerical field showed that how the tangential flow velocity increases with the increase in the ball diameters which can be caused more rise in the friction factor as confirmed in the previous results. The increase in tangential velocity is occurred near and around the outer ball diameter for all cases under analysis. Since with ball diameter enlarging, the area of mixing flow with secondary flow between fluid flow and each ball turbulators rises as a result the heat transfer also increases.

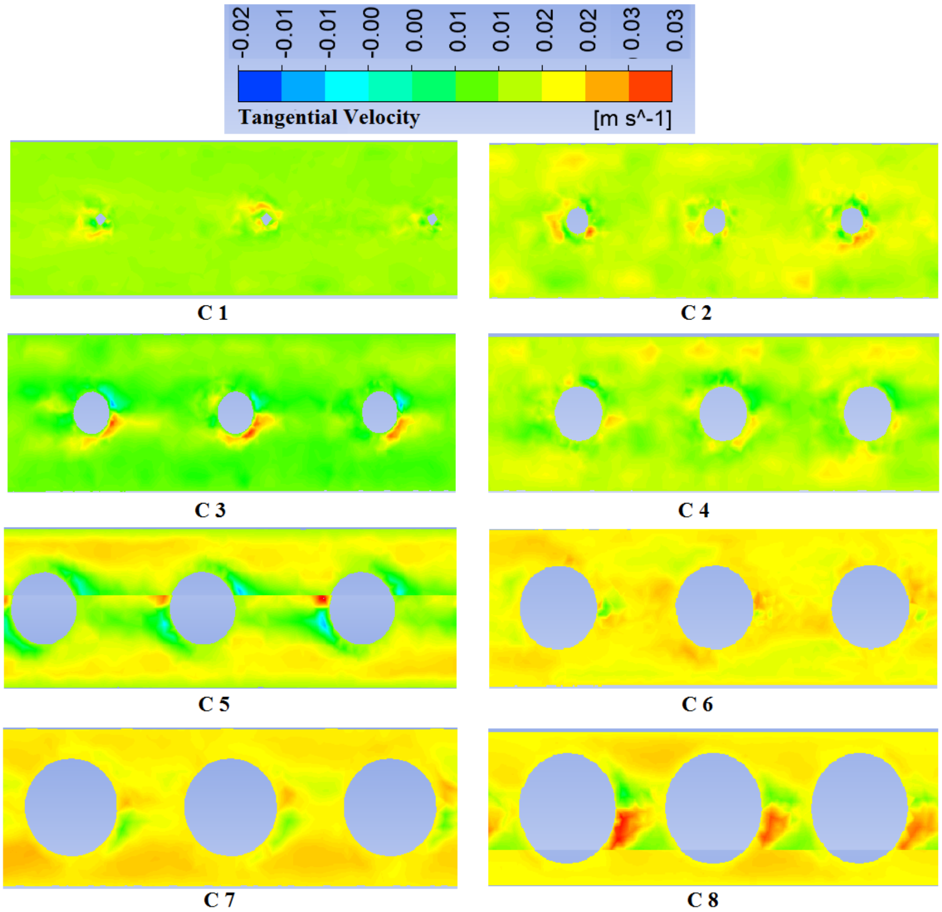

A) Tangential velocity in axial section

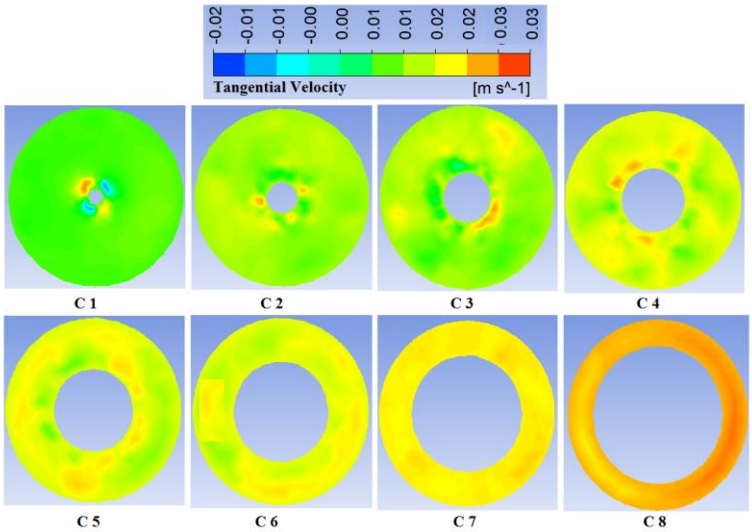

B) Radial flow direction

Figure 15: Field of tangential flow velocity in the pipe with TBI

In order to reveal the influences of the diameter of the ball on the tangential velocity, Figure 16 describes the profiles of tangential velocity. Mixing in the fluid flow, secondary flow, and more verities generation are considerably augmented when the balls are placed in the pipe which indicates positive influences of ball geometrical configurations. While, the results display good mixing influence on the fluid flow that leads to change rise in the friction factor, as well as it enhances the rate of heat transfer, and hence this result was agreed with Ref. [21].

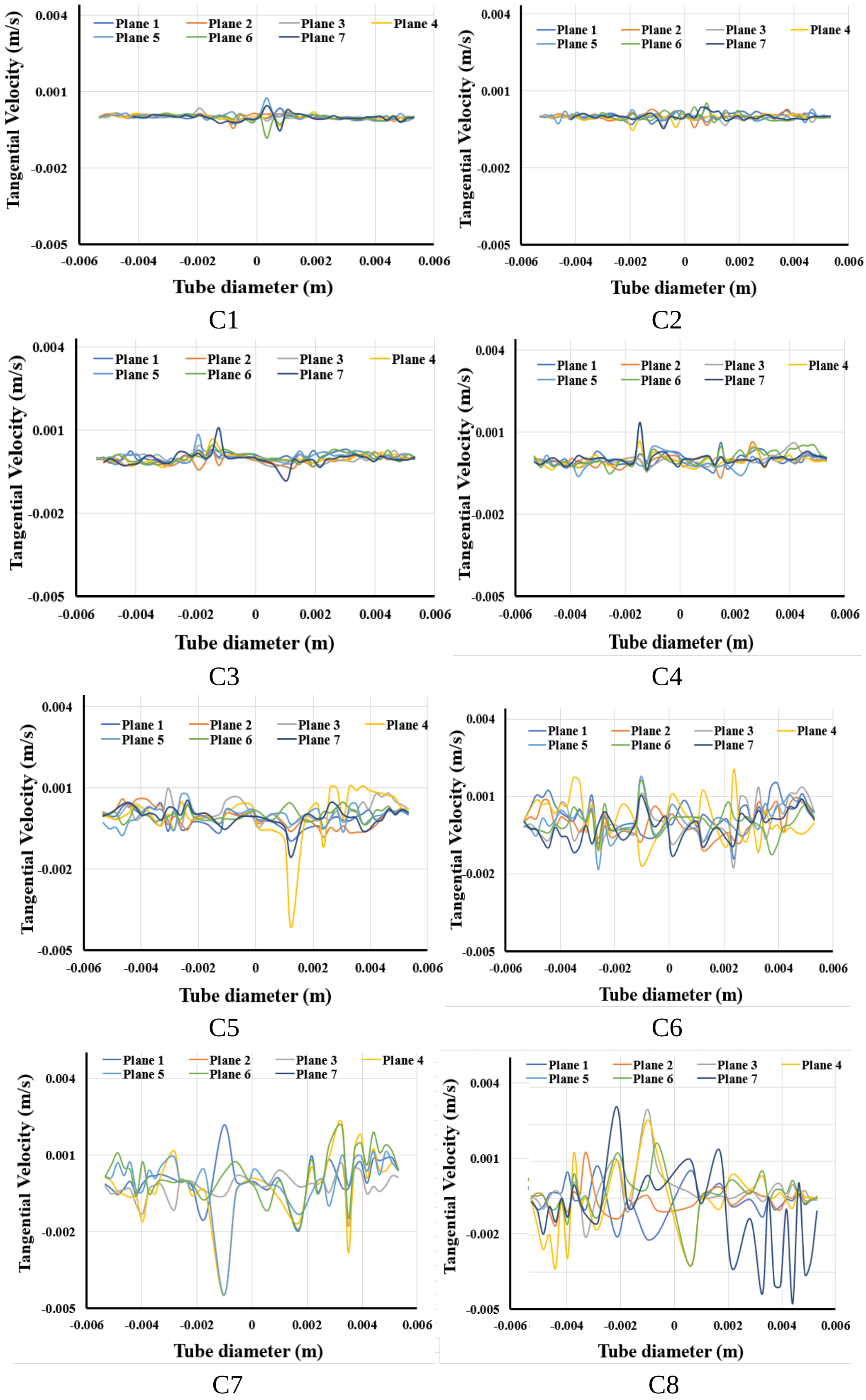

Figure 16: Change in tangential velocity profiles

The field of vorticity magnitude contours is shown in Figure 17 A and B. As noted from both figures the change in vorticity magnitude variations increases as the ball diameter incenses explicitly closed to the outer ball diameter. When the fluid flow stream moves and encounters over each ball, the fluid glides around the surface of the ball on side of the upstream thus the flow distributing in various flow directions. This flow produces more secondary flows including swirling flow motion thus lead to generating more mixing of intense turbulent regions in these regions and close to the outer ball diameters. Consequently, the heat transfer can improve as using the ball inside the pipe.

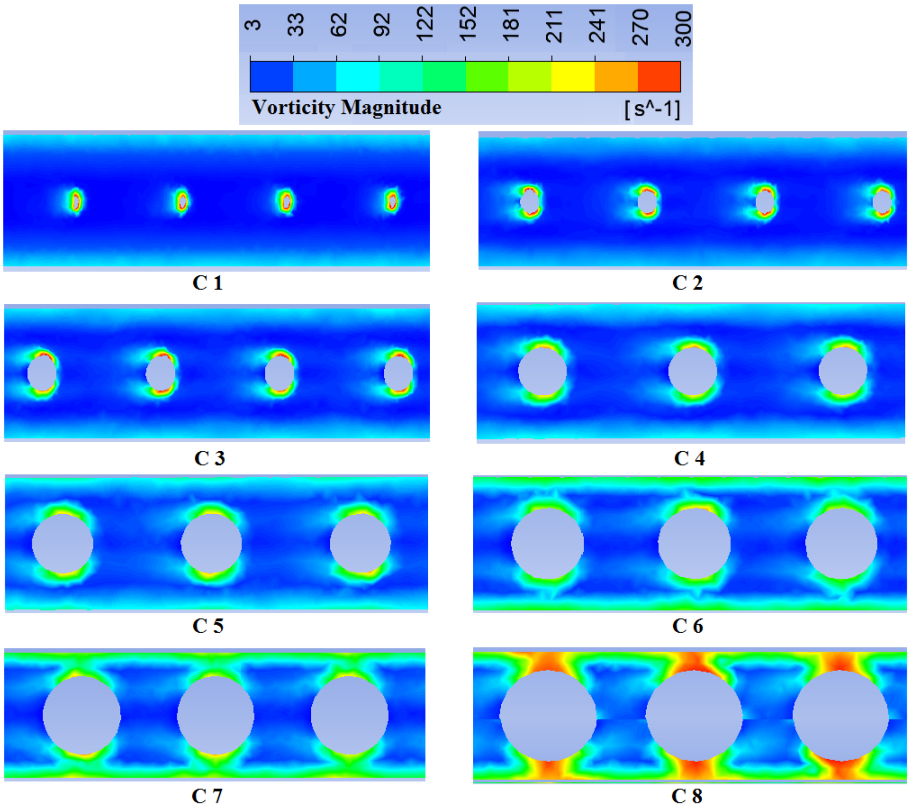

(A)

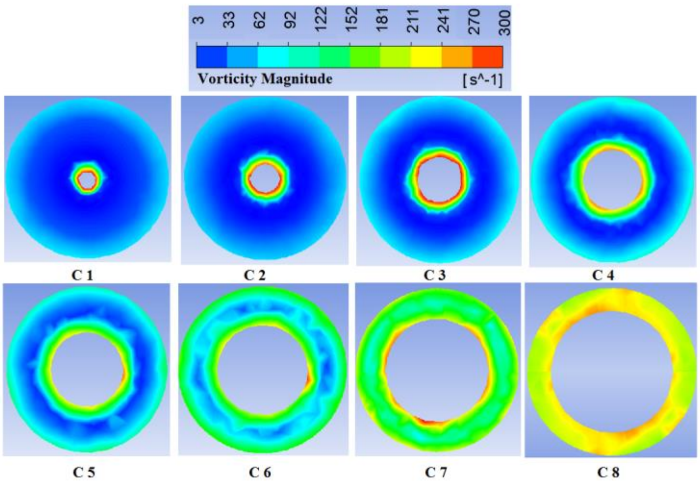

(A)

Figure 17: Variations in vorticity magnitude fields with different BTI

Figure 18 represents the change in the vorticity magnitude profiles with various BTI. It can be observed that all profile curves are non-uniform shapes and this non-uniformly increased as the ball size increased for all models under analyses. The reason for this is due to the reduction of flow area near and over each ball resulting in complex mixing flows and turbulent vortex flow. Moreover, the turbulent vortex flow near the balls caused an interaction with the main flow field, and hence this result was agreed with Refs. [21 and 22].

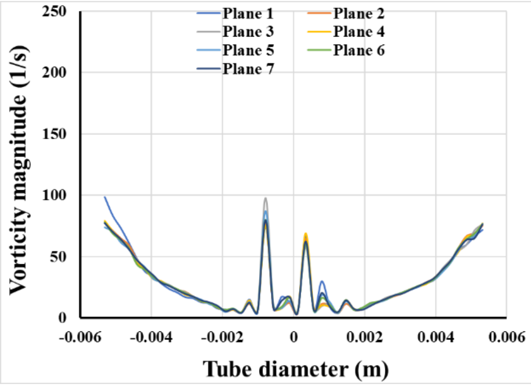

C1

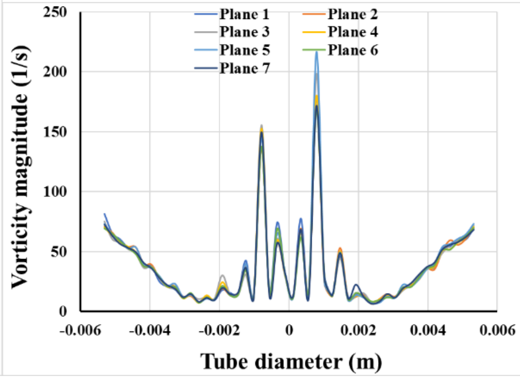

C2

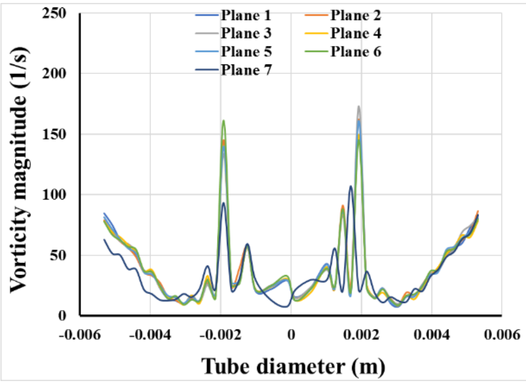

C3

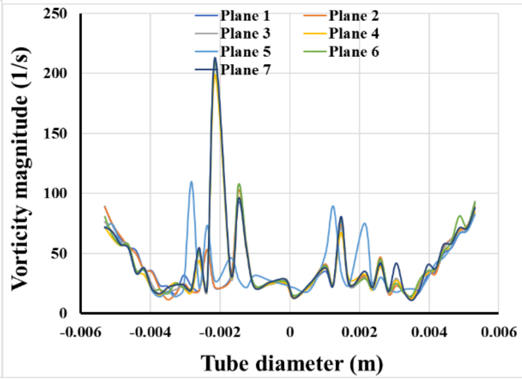

C4

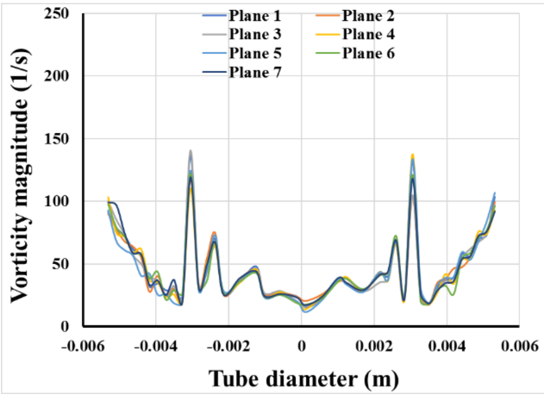

C5

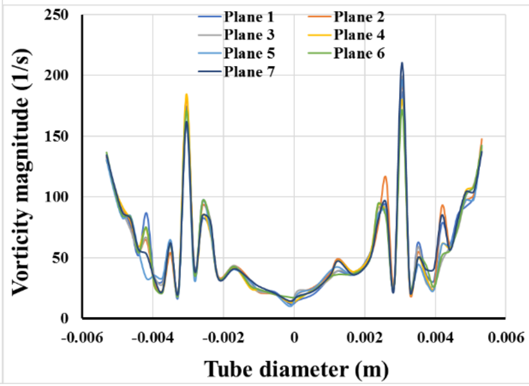

C6

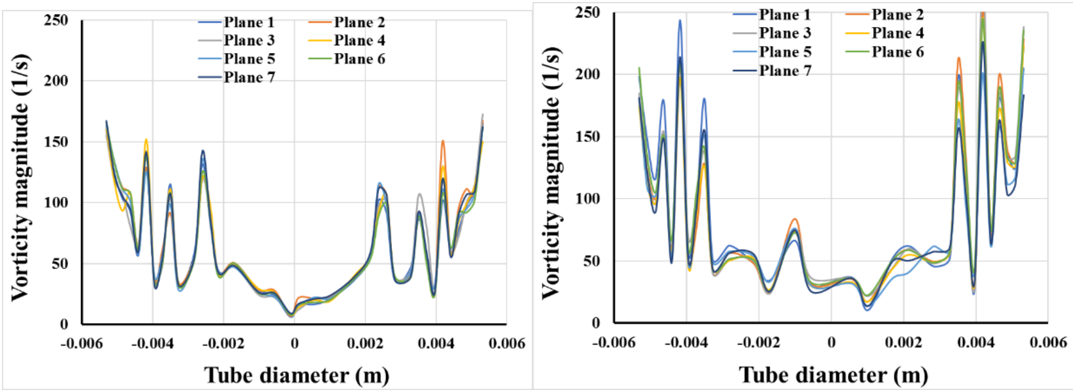

C7 C8

Figure 18: Variations in the vorticity magnitude profiles at variety of BTI

The turbulence kinetic energy (TKE) is the mean K.E per unit mass associated with eddies in a turbulent flow. This is a vital parameter within the fluid flow boundary layer. Figure 19 represents the contours of TKE fields with various BTI diameters. The results indicated that TKE increased near the ball region with significantly higher gradients appearing in the flow area between the pipe wall and the especially with the larger ball diameters. this rise of TKE gradient in the boundary layer can lead to an increase in the rate of heat transfer.

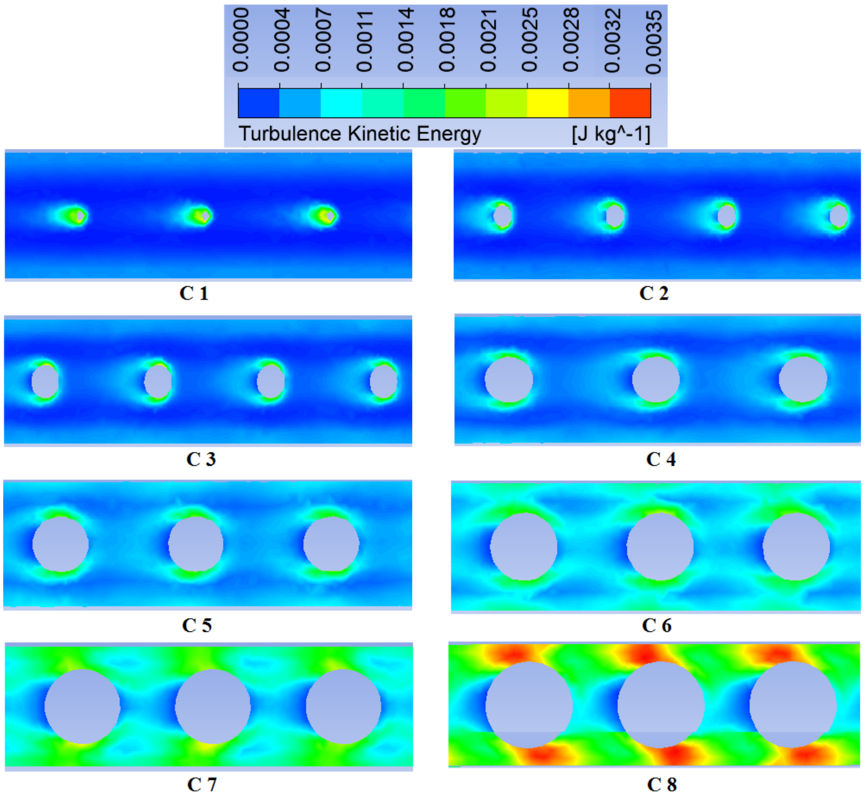

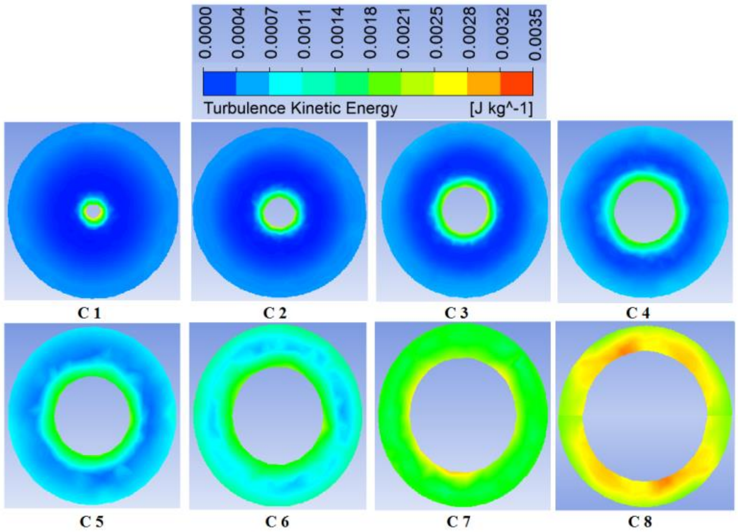

Figure 19: The change in the TKE field contours

The next diagram in Figure 20 illustrates the TKE profiles versus the BTI diameter. It can be noted that the pattern of TKE profile trend to have the same profiles as in previous figures. The shapes of these profiles are non-uniform for all curves due to the effect of ball configurations. This is possibly happened due to the rise in the intensity of mixing fluid flow. Also, using this type of ball inserts in the pipe can provide more turbulent intensity. On the other hand, the larger the ball size inserts in the pipe the more complex is the flow and that leads to more enhanced heat transfer. Based on the above finding, it can be noticed that the ball insert configurations have a high effect on flow behaviour and improvement of heat transfer in the heat exchanger pipes.

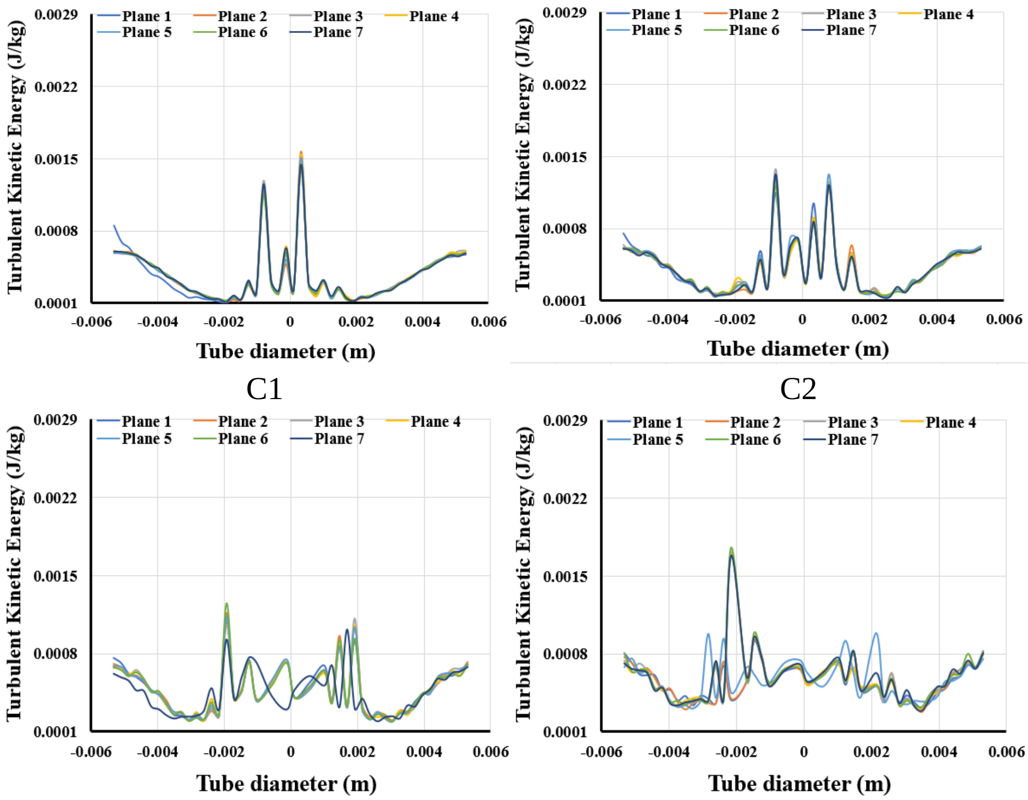

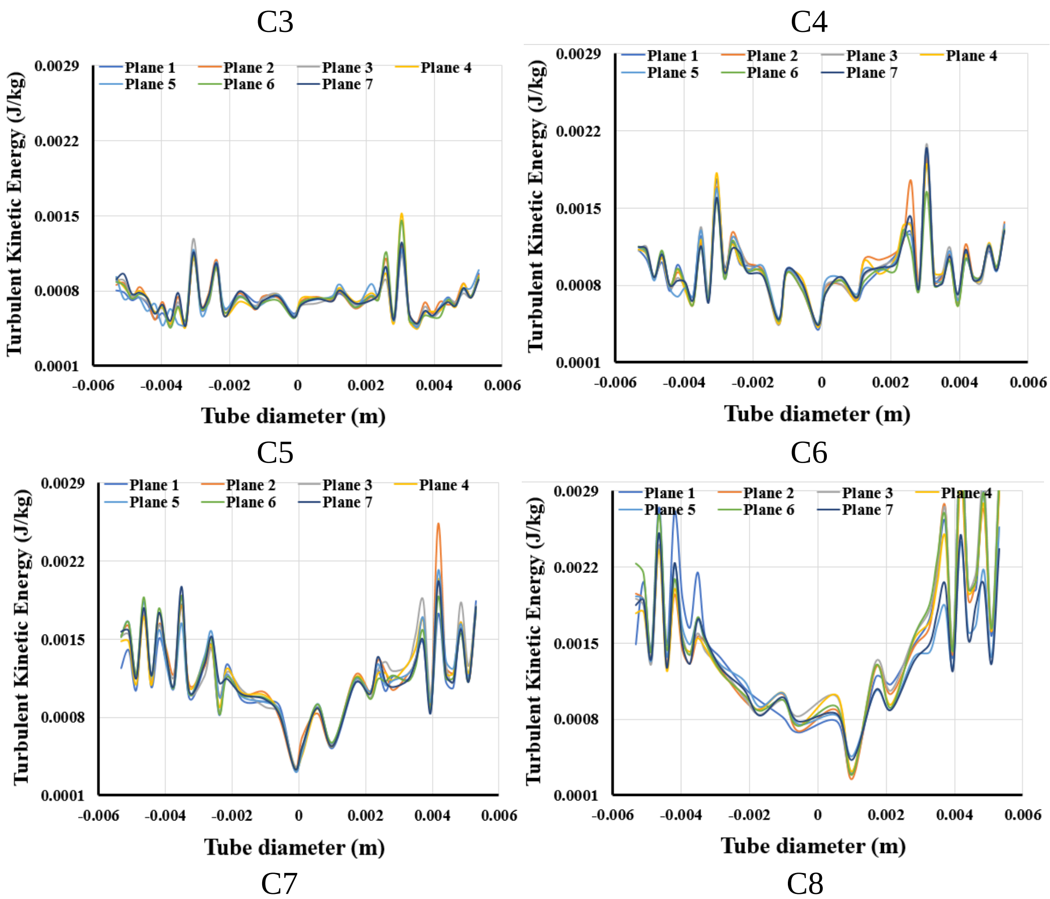

Figure 20: Variations in TKE profiles

The influence of using the ball turbulators with various diameters on the turbulent viscosity is presented in Figure 21. From this figure, the numerical investigation revealed that the turbulent viscosity happened for the insert balls with bigger diameter. The effect of swirling flow in the region of inter-ball has maximum velocities that lead to cause more mixing of intense turbulent in the fluid flow. This flowing stream can hit the ball upstream side at high velocities thus generating flow impingement influence which subsequently caused a rise in the level of turbulence near the upstream region of the balls. A higher level of turbulence viscosity can be seen in the region between balls. This due to the mixing of the main fluid and the secondary flows backing from the ball side upstream as well as the flow acceleration in the constricted region.

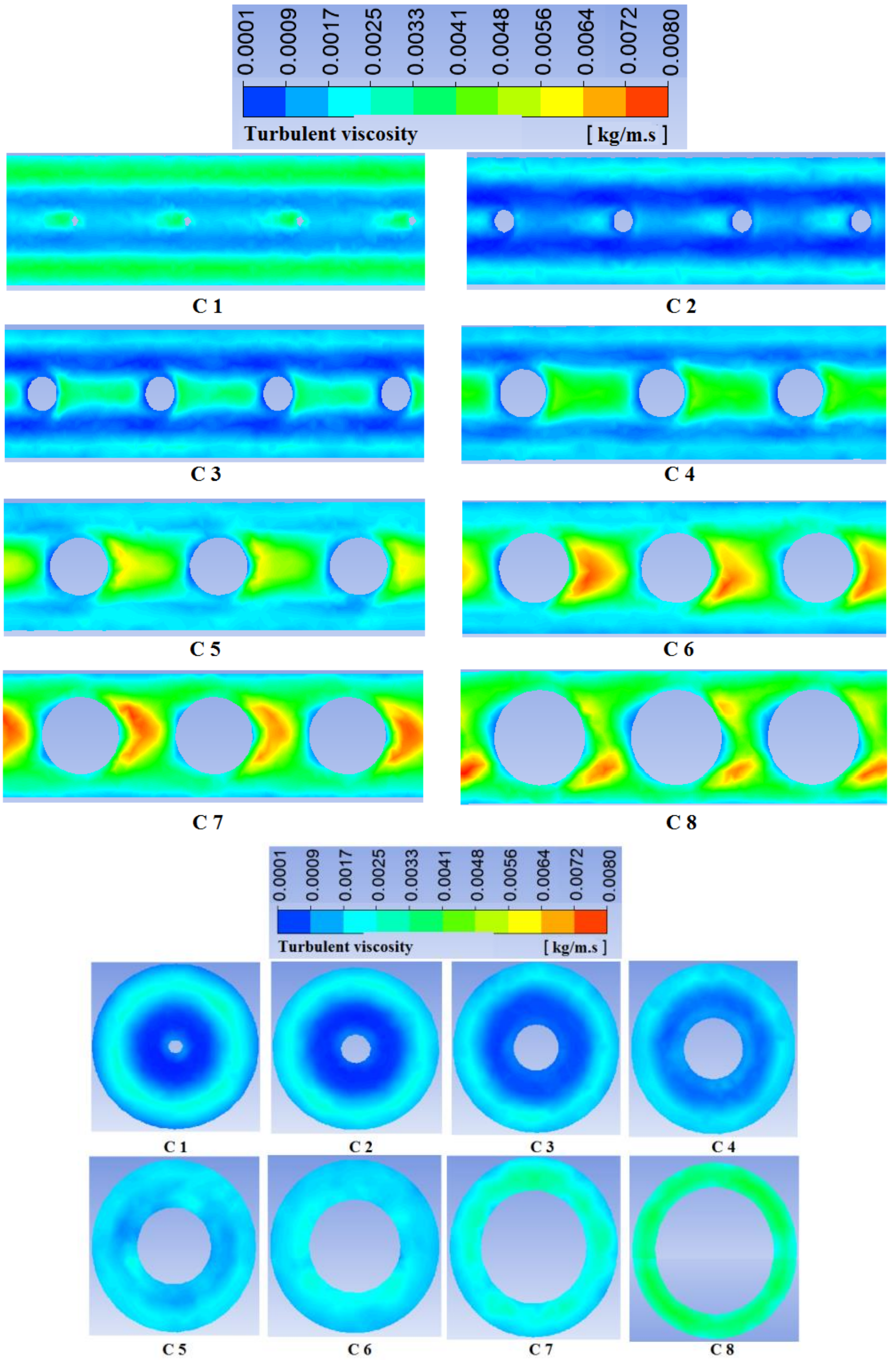

Figure 21: Turbulent viscosity variations fields with various of BTI

Figure 22 describes the turbulent viscosity profiles with different BTI. It can be noted that the ball configurations have more effect on the value and shape of all turbulent viscosity profiles as observed in this figure because of the same above reasons in the previous figure.

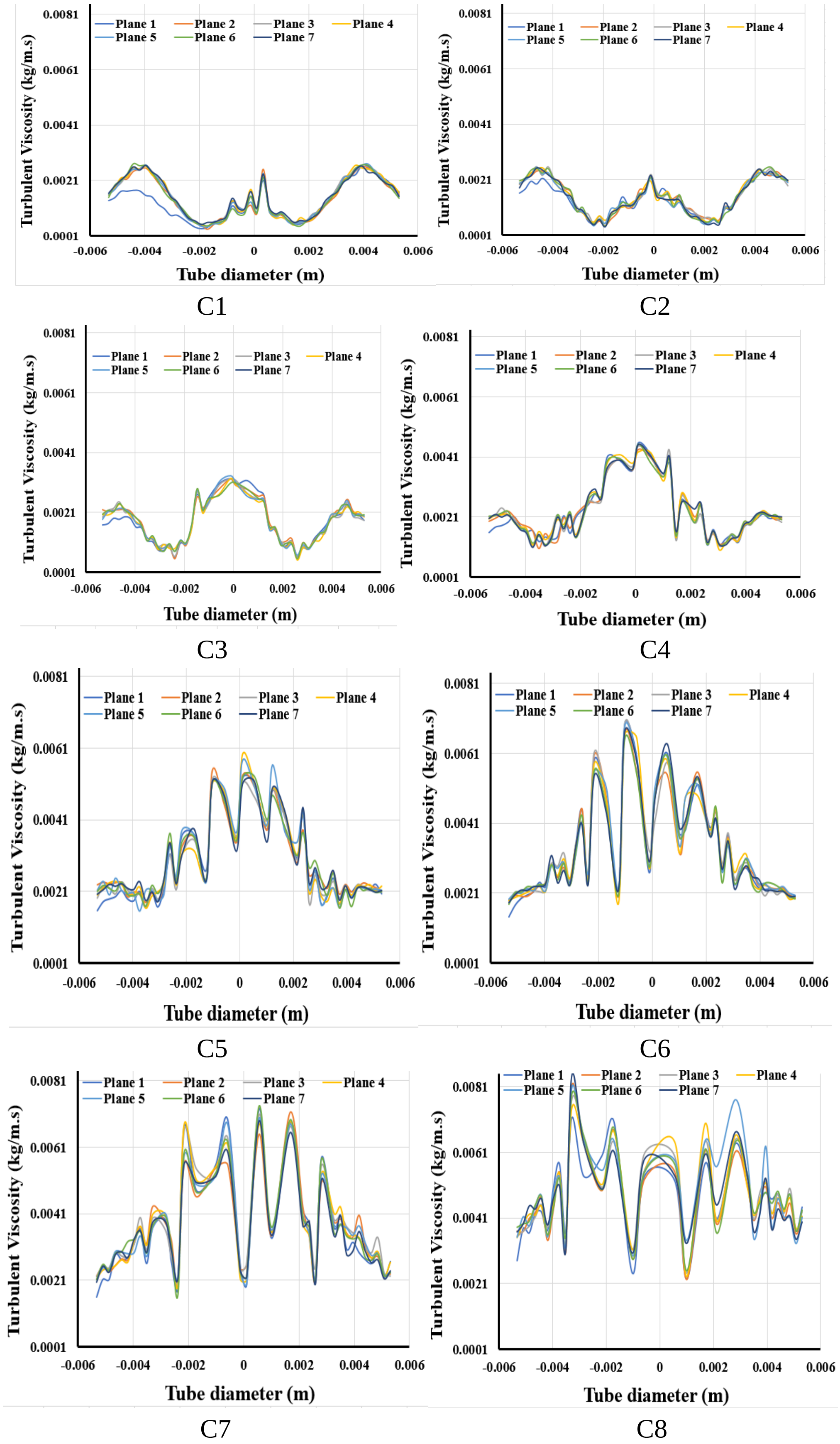

Figure 22: Turbulent viscosity variations profiles with variety of BTI configurations

4.2. Thermal Performance Analysis

Figure 23 illustrates the temperature field in the pipe obtained from the numerical modelling. As could be seen from the figure the temperature decreases as the pipe length increases. The higher temperature takes place closed to the inlet plane as expected and the lower temperature occurs at the outlet pipe plane.

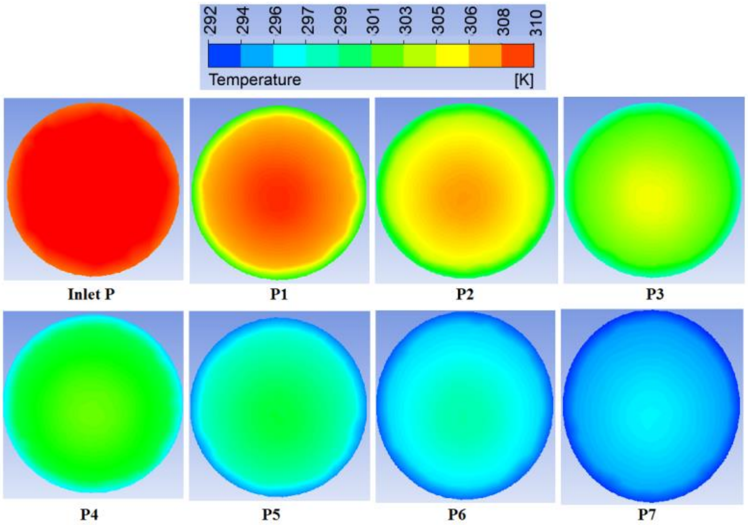

Figure 23: The change in static temperature at different planes

Figure 24 represents curves of static temperature profiles, the result revealed that as the ball diameter increases the shape of profiles becomes more non-uniform as seen in this figure. Also, as the ball diameter increase, the thermal boundary layers change and become thinner due to the disturbance in the boundary layer and mixing fluid flow. It can be observed that close to the wall the temperature profiles are arranged and situated. However, in the stream turbulence region, the mixing layers take place and this happened due to the vortices interaction. Meanwhile, the convective heat transfer can effectively be enhanced at a higher level of turbulence flow, thus improved heat transfer effectiveness.

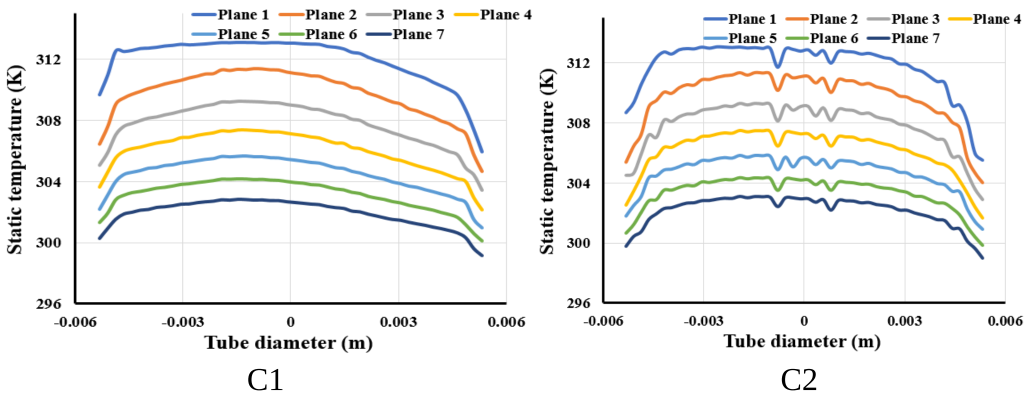

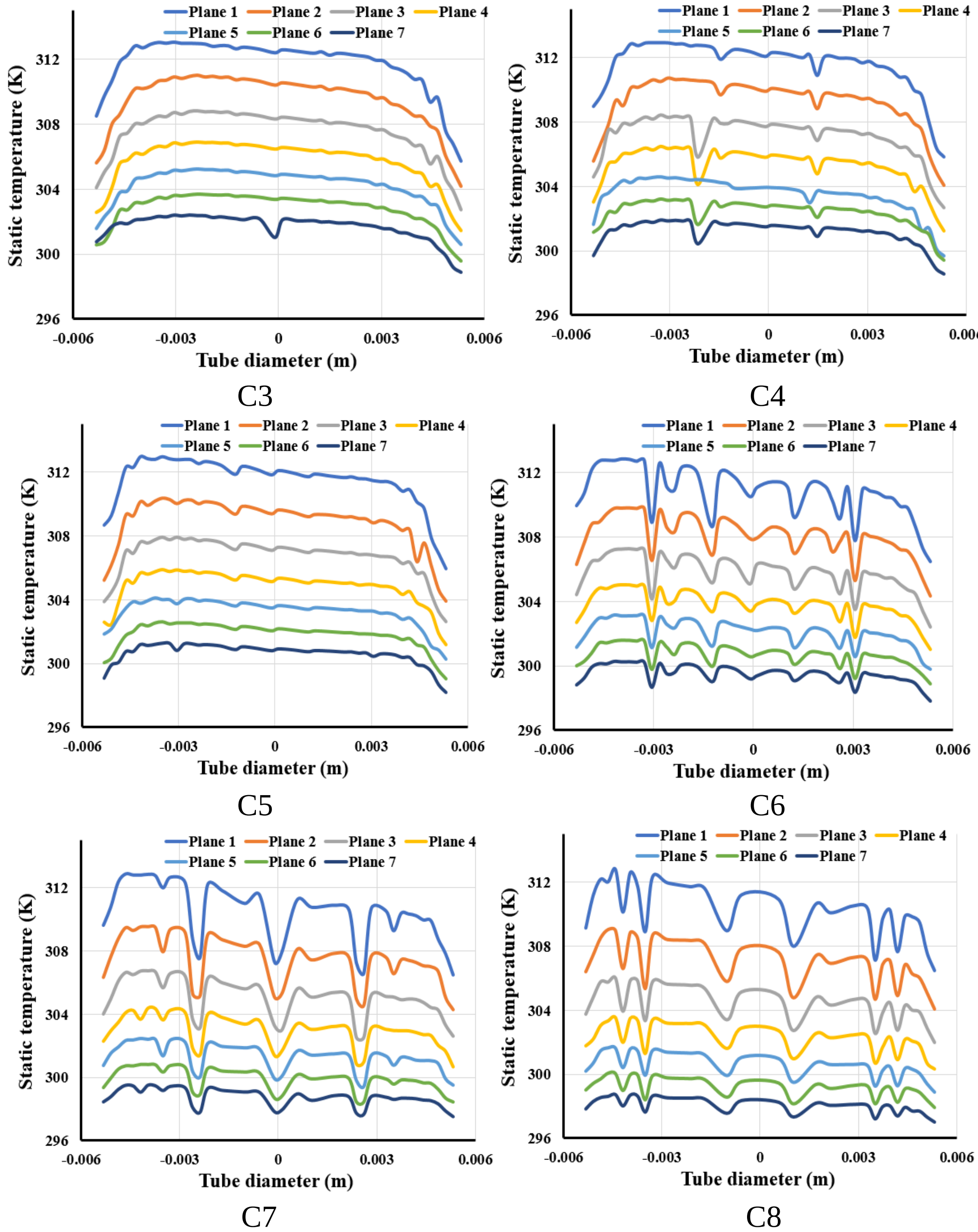

Figure 24: Differences in static temperature at various BTI

4.3. Analysis the Flow Behaviour along the Flow Direction in the Pipe

In order to investigate the fluid flow along the pipe length with and without BTI two test lines are used for this analyses purpose as illustrated in Figure 25.

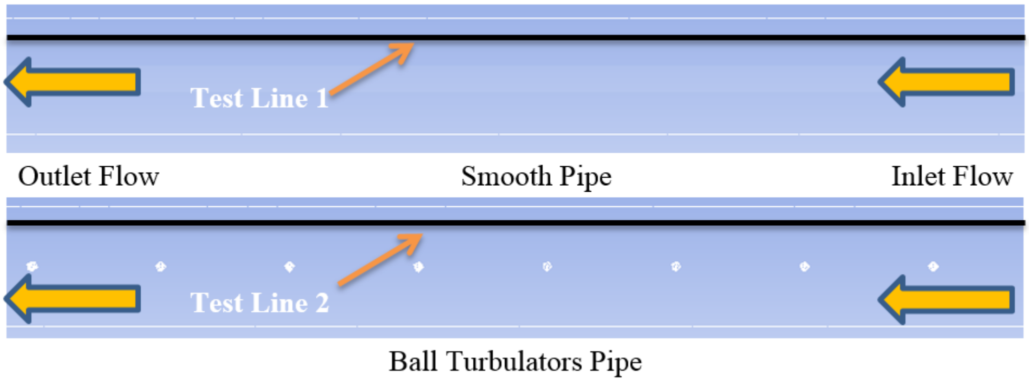

Figure 25: Using different lines test for the flow behaviour in the pipe

Figure 26 A represents the effect of BTI diameters on the pressure drop along with flow direction in the pipe using two test lines (line 1 and line 2). The results revealed that the BTI has a higher influence on the pressure drop across the pipe. As expected increase in the BTI diameters caused a rise in the pressure. Moreover, it can be noted that as the pipe length increases the pressure decreases for all cases in this figure. The value of pressure drop using BTI is higher than that without BTI. This happened due to several reasons including the flow resistance between the main flow direction and the ball inserted, the flow mixing and the increase in shear stress as well as due to vortex and swirl flows. Figure 26 B illustrates the variations in dynamic pressure along the total pipe length for different BTI configurations. It is evidently noted that when the BTI diameter increases that lead to dynamic pressure increases and the maximum value of dynamic pressure takes place at a bigger BTI diameter. Moreover, this change in dynamic pressure inside the pipe was as sinusoidal waves for all cases under analyses.

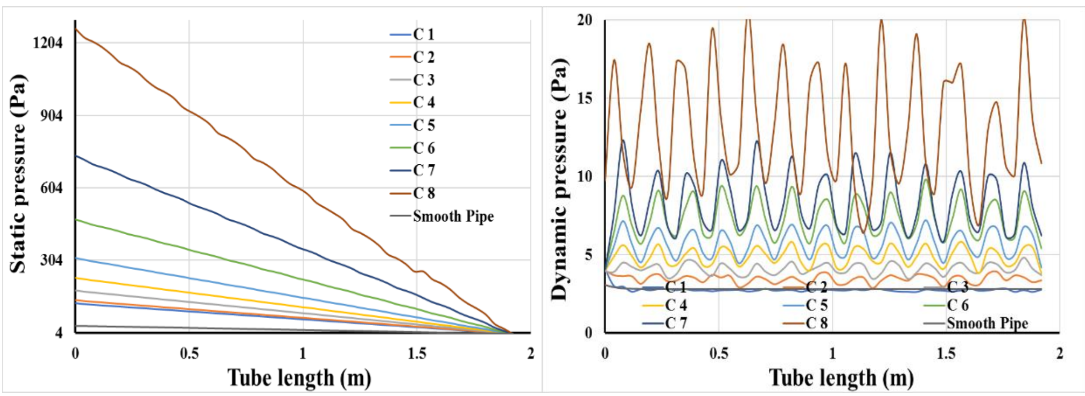

A) Static pressure B) Dynamic pressure

Figure 26: Analysis static and dynamic pressure using two test lines

For more information regarding the flow behaviour, Figure 27 describes the vorticity magnitude and different velocity components including (axial, radial, and tangential). As noticed that all above parameters are highly affected due to position the BTI in the pipe. Also, the value and shape of all parameters are changed and increased as the BTI configurations increased. This happened due to the same above reason mentioned in the previous figure. Furthermore, this rise in the velocity components gradients can change in the boundary layer then leads to bringing an increase in the heat transfer and hence an improvement of overall heat transfer rate. Based on the above findings it can be found that the BTI has more influence on all of the flow fields in the pipe.

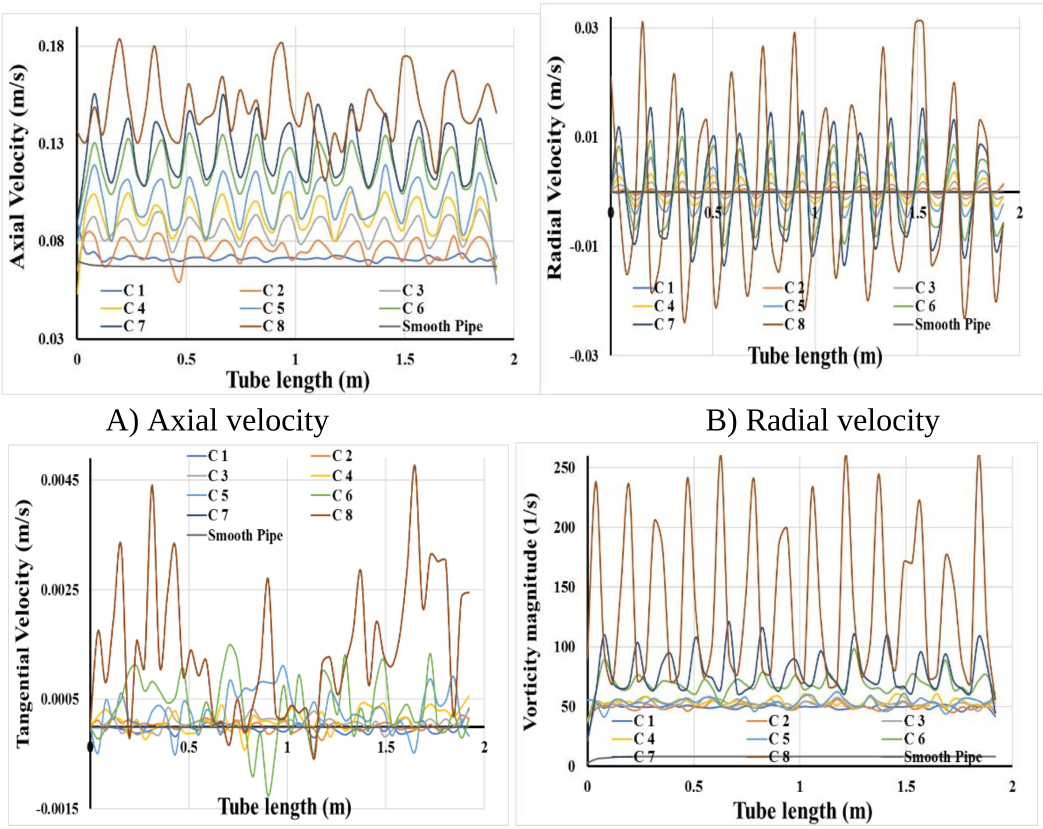

A) Axial velocity

B) Radial velocity

C) Tangential velocity

D) Vorticity magnitude

Figure 27: Variations in the different velocity components in the pipe

More investigation can be shown in Figure 28 for variations in the TKE and Turbulent viscosity curves in the total pipe length with a variety of BTI. As observed that the value of TKE and Turbulent viscosity incenses when the BTI incenses. Also, the value of latter parameters using BTI are higher than smooth pipe. Additionally, results revealed that the pipe with BTI can increase temperature fluid flow, which raises the gradient of temperature between the fluid flow and pipe wall side subsequently brings a enhance the rate of heat transfer.

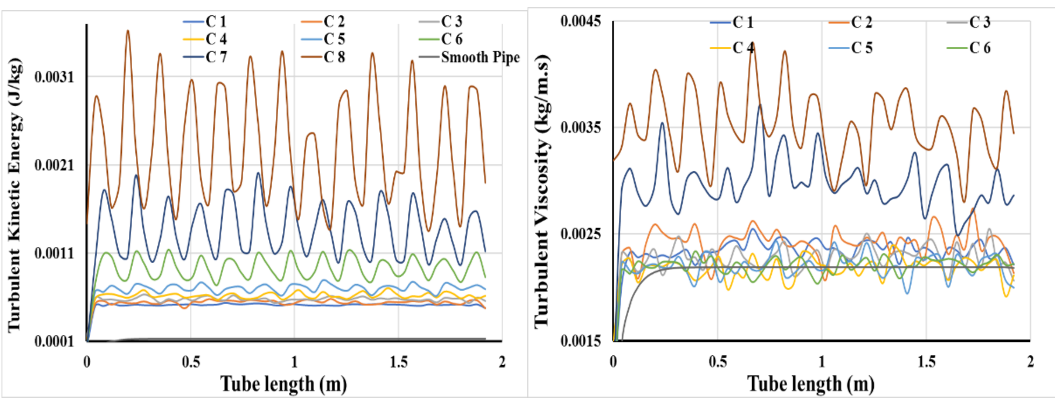

A) TKE B) Turbulent viscosity

Figure 28: TKE and Turbulent viscosity variations along the total pipe flow direction

The last important Figure shows the change in the static temperature by using different BTI diameters across the total pipe length. It is clearly noticed that the trend of temperature for all cases under study are gradually decreased as the total pipe length increased as expected. Moreover, as the BTI diameters increased the improvement of heat transfer performance also increased as listed in Table 2. By analysing this table, it can be found that as compared with smooth tube it can be found that the use of BTI can enhances the rate of heat transfer performance more than 46.85%. According to these results it can be noted that BTIs have highly effect on the increases temperature in the pipe and increases the surface area the improve the heat transfer.

Table 2: The effect of using BTI on temperature difference (ΔT)

Case	Without BTI	C 1	C 2	C 3	C 4	C 5	C 6	C 7	C 8
ΔT (K)	8.94	11.69	13.10	13.15	13.52	14.05	14.98	15.84	16.82
Percentage differences (%)	(-)	23.52	31.75	32.01	33.88	36.37	40.32	43.56	46.85
$\Delta P/L$ (Pa/m)	0.0166	0.066	0.072	0.093	0.1209	0.163	0.246	0.384	0.673

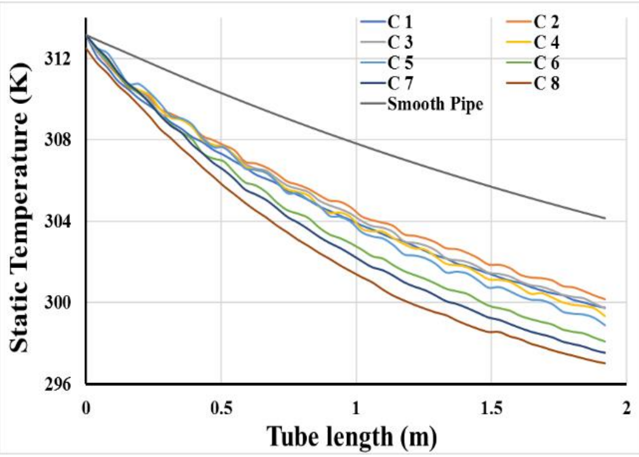

Figure 28: Variations in the temperature differences across the total pipe length with and without BTI

4.4. Evaluation of the heat transfer performance

Numerical outcomes reflect the heat transfer performance, as well as the overall heat transfer, which is analysed according to the different ball turbulators inserts (BTI). Influence of the BTI with several geometrical configurations on heat transfer performance is exhibited in Figure 29. It can be observed that from Figure 29 (a) the friction factor (f) is highly affected due to the BTI inside the pipe and the f increases as the BTI diameter increases that happened because of the increase in pressure drop in the pipe. The results indicate that the high value of the f is at the high BTI diameter.

Figure 29 (b) shows the effect of BTI on Nusselt number. As seen that the Nusselt number decreases as the BTI geometrical configuration increase in the pipe. Due to the increase, the pressure drop in the pipe.

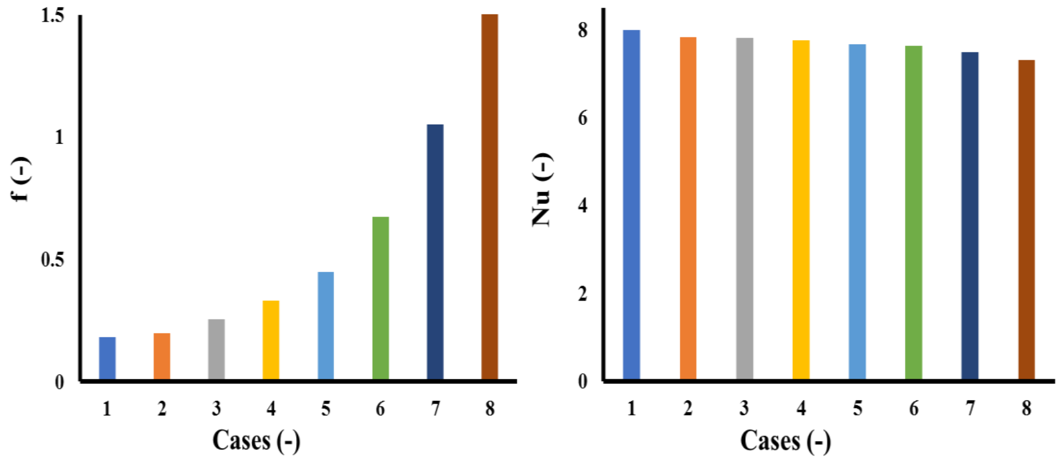

(a) (b)

Figure 29: The relationship between the friction factor and Nusselt number with different BTI

As obviously observed from Figure 30 (a) and (b) the friction factor with BTI over friction factor without BTI ratio (f/fo) and the ratio of Nusselt number with BTI over Nusselt number without BTI ratio (Nu/Nuo) have same trends in Figure 29 (a) and (b) for the f and Nu.

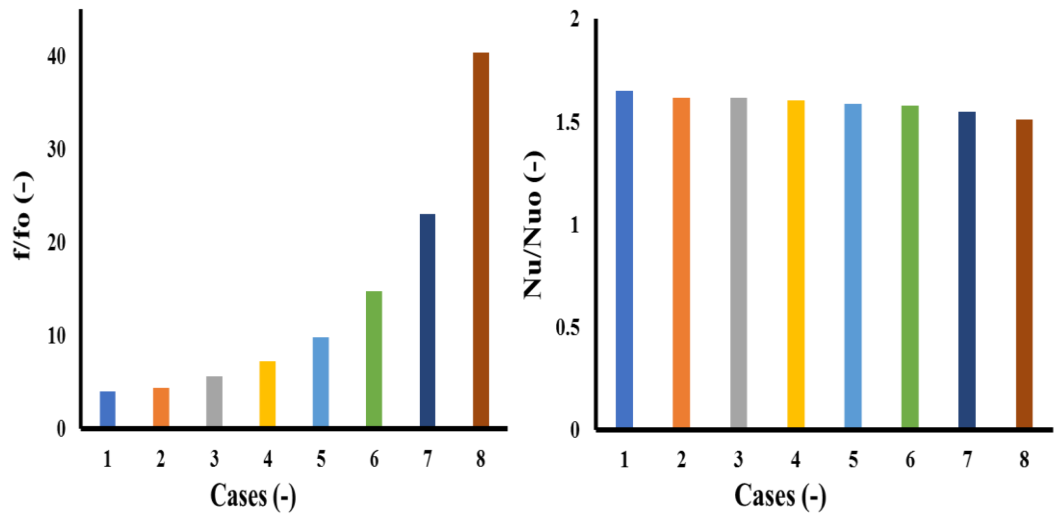

(a) (b)

Figure 30: The relationship between the f/fo and Nu/Nuo with different BTI

Figure 31 represented performance of the overall heat transfer (PEF) with different BTI geometrical parameters. As obviously noted from this figure the tends of PEF is decreased as the BTI increase. Additionally, the dropped slope mostly decreases. Moreover, the maximum value for the PEF is found to be more than 1.03. It is evident that the value of PEF is affect by BTI. Furthermore, clear that the values of PEF are higher than 1 as the BTI diameters decreased. Since the above investigation, it low BIT diameters are chosen to enhance the heat exchange.

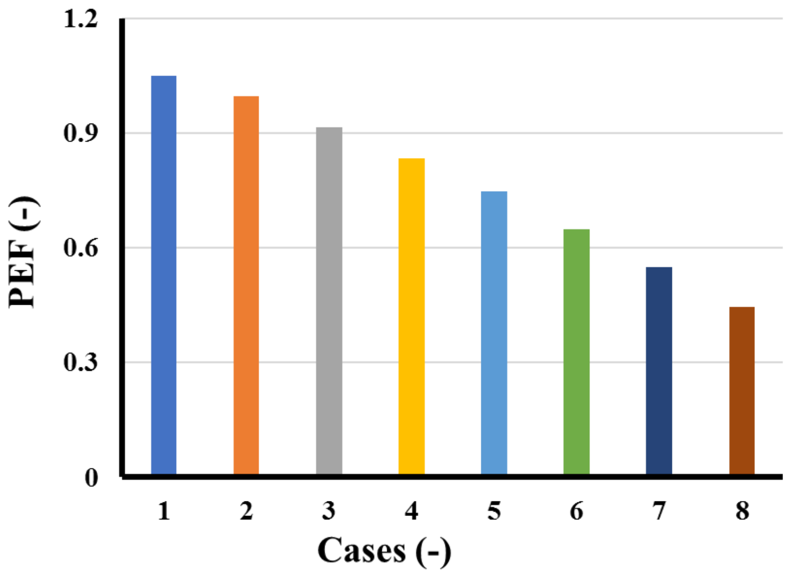

Figure 31: The performance evaluation factor with different BTI configurations

5. Conclusions

The flow behaviour, pressure drop, thermo-hydraulic characteristics, and enhancement in a three dimensions circular pipe with and without ball turbulators inserts (BTI) are investigated using CFD numerical calculations. Based on this study different conclusions can be noted as following:

1. The value of pressure in the pipe with ball increases as the ball diameter incenses and the maximum pressure value take place at case C 8 with ball diameter of 8 mm. Due to location of these balls can cause more mixing flow and generate more vortex flow and hence that lead to attribute the destruction in thermal boundary layer.
2. Maximum dynamic pressure seems near the pipe wall area instead of the central pipe area. This increase in dynamic pressure gradient can affect inducing the distribution of intense flow due to cause more mixing flow and hence leads to enhance the heat transfer rate between the flowing liquid and the pipe wall regions.
3. The value of velocity increases around and between the outer ball diameter and the pipe wall regions. This change in velocity leads to a higher flow resistance in flow direction then in the boundary layer the velocity gradient also increases.
4. The influence of BTI configurations is greatly disturbed and intensified the boundary layer and as the ball diameter increase the relevant intensity rises.
5. Results also indicated that the TKE gradient increases near the outer ball diameter especially near the distance between the ball and pipe wall and it is increased as the ball diameter increases.

6. The velocity fields contours, it is revealed that the characteristics of flow behaviour are closely associated with the BTI. Also, the computation results indicated that the fluid flow velocity nearby the pipe wall and around the BTI is importantly enhanced, as compared to without BTI in the same conditions is used.
7. Using BTI presented a distinguished influence on the rate of heat transfer. Formation of more vortex flow through means of this kind of BTI is a important parameter in the enhancement of heat transfer. Use of BTI can enhances the rate of heat transfer performance more than 46.85%.
8. The result revealed that using the CFD visualization method to analyse the flow characteristics and heat transfer can offer more details regarding the distribution in a fluid flow which is difficult to obtain in experimental approaches.
9. The results noted that the maximum value for the PEF is found to be more than 1.03.

Acknowledgments

The author of this present work would like to thank Mustansiriyah University (www.uomustansiriyah.edu.iq) Baghdad – Iraq for its support.

Author ORCID ID

Dr. Ahmed Ramadhan Al-Obaidi
https://orcid.org/0000-0003-3819-7008

Compliance with Ethical Standards:

Funding: This study was no funded.

Conflict of Interest: Authors have not received any research grants: The authors declare that they have no conflict of interest.

References

[1] Liang, C., Tong, X., Lei, T., Li, Z., & Wu, G. (2017). Optimal design of an air-to-air heat exchanger with cross-corrugated triangular ducts by using a particle swarm optimization algorithm. Applied Sciences, 7(6), 554.

[2] Bergles, A. E. (2002). ExHFT for fourth generation heat transfer technology. Experimental Thermal and Fluid Science, 26(2-4), 335-344.

[3] Chowdhury, M. K., Bhuyan, M. M., & Deb, U. K. (2019). Augmentation of Heat Transfer in Pipe Flow Using Plain Twisted Tape Inserts for Different Twist Ratios. Energy and Power Engineering, 11(9), 342-354.

[4] Bahiraei, M., Mazaheri, N., & Aliee, F. (2019). Second law analysis of a hybrid nanofluid in tubes equipped with double twisted tape inserts. Powder technology, 345, 692-703.

[5] Naterer, G. F. (2003). Heat transfer in single and multiphase systems. CRC press. Printed in the United States of America.

[6] Ewing, J. A. (2015). Thermodynamics for engineers. Cambridge University Press. UK.

[7] Bejan, A. (2013). Convection heat transfer. John wiley & sons. UK.

[8] Singh, P., Pandit, J., & Ekkad, S. V. (2017). Characterization of heat transfer enhancement and frictional losses in a two-pass square duct featuring unique combinations of rib turbulators and cylindrical dimples. International Journal of Heat and Mass Transfer, 106, 629-647.

[9] Bianchini, A., Balduzzi, F., Bachant, P., Ferrara, G., & Ferrari, L. (2017). Effectiveness of two-dimensional CFD simulations for Darrieus VAWTs: a combined numerical and experimental assessment. Energy Conversion and Management, 136, 318-328.

[10] Al-Obaidi, A. (2018). Experimental and Numerical Investigations on the Cavitation Phenomenon in a Centrifugal Pump (Doctoral dissertation, University of Huddersfield).

[11] Al-Obaidi, A. R. (2019). Monitoring the performance of centrifugal pump under single-phase and cavitation condition: A CFD analysis of the number of impeller blades. J. Appl. Fluid Mech, 12(2), 445-459.

[12] Al-Obaidi, A. R. (2019). Effects of different turbulence models on three-dimensional unsteady cavitating flows in the centrifugal pump and performance prediction. International Journal of Nonlinear Sciences and Numerical Simulation, 20(3-4), 487-509.

[13] Patil, P., & Deshmukh, P. (2014). An experimental study of heat transfer enhancement in the circular channel with almond shape dimples. IOSR Journal of Mechanical and Civil Engineering (IOSR-JMCE), 11, 48-57.

[14] Hosseinnejad, R., Hosseini, M., & Farhadi, M. (2019). Turbulent heat transfer in tubular heat exchangers with twisted tape. Journal of Thermal Analysis and Calorimetry, 135(3), 1863-1869.

[15] Abraham J, & Maki R. (2018). Hydrodynamics of laminar flow through dimpled pipes. MOJ Civil Eng.;4(3):150–154. DOI: 10.15406/mojce.2018.04.00113.

[16] Vignesh, S., Moorthy, V. S., & Nallakumarasamy, G. (2017). Experimental and CFD Analysis of Concentric Dimple Tube Heat Exchanger. Int J Emerg Technol Eng Res (IJETER), 5(7), 18-26.

[17] Promthaisong, P., Jedsadaratanachai, W., & Eiamsa-Ard, S. (2018). Effect of geometrical parameters on turbulent flow and heat transfer behaviors in triple-start

corrugated tubes. Journal of Thermal Science and Technology, 13(1), JTST0008-JTST0008.

[18] Van Cauwenberge, D. J., Dedeyne, J. N., Van Geem, K. M., Marin, G. B., & Floré, J. (2018). Numerical and experimental evaluation of heat transfer in helically corrugated tubes. AIChE Journal, 64(5), 1702-1713.

[19] Akansu, S. O. (2006). Heat transfers and pressure drops for porous-ring turbulators in a circular pipe. Applied Energy, 83(3), 280-298.

[20] Sharma, K. K., Pradesh, M., & Tiwari, A. C. (2018). CFD based heat transfer analysis in circular tube with different orientation of insert for laminar flow. International Journal of Advance Research, Ideas and Innovations in Technology.

[21] Yuan, W., Fang, G., Zhang, X., Tang, Y., Wan, Z., & Zhang, S. (2018). Heat Transfer and Friction Characteristics of Turbulent Flow through a Circular Tube with Ball Turbulators. Applied Sciences, 8(5), 776.

[22] Afshari, F., Zavaragh, H. G., & Di Nicola, G. (2019). Numerical analysis of ball-type turbulators in tube heat exchangers with computational fluid dynamic simulations. International Journal of Environmental Science and Technology, 16(7), 3771-3780.

[23] Al-Obaidi, A. R. (2019, July). Numerical Investigation of Flow Field Behaviour and Pressure Fluctuations within an Axial Flow Pump under Transient Flow Pattern Based on CFD Analysis Method. In Journal of Physics: Conference Series (Vol. 1279, No. 1, p. 012069). IOP Publishing.

[24] Omidi, M., Darzi, A. A. R., & Farhadi, M. (2019). Turbulent heat transfer and fluid flow of alumina nanofluid inside three-lobed twisted tube. Journal of Thermal Analysis and Calorimetry, 1-12.

[25] Albanesi A. W., K. D. Daish B. Dally and R. C. Chin (2018). Investigation of heat transfer enhancement in dimpled pipe flows. 21st Australasian Fluid Mechanics Conference Adelaide, Australia.

The Nomenclature

3D	Three dimensions
BTI	Ball Tabulators Inserts
CFD	Computational Fluid Dynamics
C_p	Specific heat coefficient
D	Pipe diameter
d_e	Pipe effective diameter
fo	Smooth pipe friction factor
h	Heat transfer coefficient
i, j, k,	Velocity directions in X, Y and Z
k	Fluid thermal conductivity

L	Pipe length
$\dot{m}_w$	Mass flow
Nuo	Smooth pipe Nusselt number
P	Pressure
PEF	Performance Evaluation Factor
t	Time
T	Temperature
Tb	Bulk temperature
TKE	Turbulent kinetic energy
Tin	Inlet temperature
Tout	Outlet temperature
v	Flow velocity
U	Fluid velocity
ρ	Density
μ	Dynamic viscosity